A Fiftieth Year Retrospective on the 1976 M_W 7.5 Motagua Earthquake in Guatemala

Grant Clark[1], Trenton McEnaney[1], Jeremy Maurer[1], Andreas Eckert[1], Stephen S. Gao[1], Omar G. Flores[2], Robin Yani[3], Tina Niemi[4], Christoph Grützner[5], Francisco Gomez[6], and Jonathan Obrist-Farner*[1]

ABSTRACT

On 4 February 1976, an $M_w > 7.5$ earthquake ruptured ~240 km of the Motagua fault in Guatemala, causing ~23,000 fatalities. This event provided evidence for the fault's role as a major transform boundary between the North American and Caribbean plates. Field observations, seismological analyses, and postseismic studies helped constrain fundamental aspects of the 1976 earthquake mechanics and the spatial complexity of the rupture. This event opened a window for studies documenting past deformation along this plate boundary across multiple spatial and temporal scales. Five decades of research have established this earthquake as an important event for understanding strike-slip ruptures along major plate boundaries. This review integrates legacy field observations, subsequent analyses, and recent investigations along the North American and Caribbean plate boundary in Guatemala. Our goal is not only to synthesize the details and highlight the importance of the event but also to preserve essential datasets that continue to inform our understanding of plate boundary mechanics, seismic hazard, and the long-term behavior of this major transform fault system.

KEY POINTS

- We review and summarize 50 yr of research on the 1976 $M_w > 7.5$ Motagua earthquake.
- Legacy datasets provide unprecedented documentation of the rupture and effects of the earthquake.
- Poor monitoring and uncertain earthquake recurrence leave Guatemala vulnerable to future large earthquakes.

INTRODUCTION

On 4 February 1976, a devastating $M_w > 7.5$ strike-slip earthquake occurred along the left-lateral Motagua fault in Guatemala. The Motagua fault is part of the Polochic–Motagua fault system and is the primary fault along the North American and Caribbean plate boundary in Guatemala (Lyon-Caen *et al.*, 2006; Fig. 1). The earthquake had both significant societal and scientific impacts.

From a societal point of view, the 1976 Motagua fault earthquake generated a ~240 km surface rupture (Fig. 1b) and resulted in ~23,000 fatalities, >76,000 injuries, and >1.2 million displaced persons. Before the earthquake, no building codes had been implemented for earthquakes (Husid *et al.*, 1976). Most of the adobe structures in the vicinity of the rupture and along its western terminus were completely destroyed (Fig. 2). Several reinforced-concrete structures in Guatemala City also collapsed, resulting in the majority of human casualties. Guatemalan society in general was also affected by the collapse of bridges, roads, and railroad tracks and by extensive landslides and soil liquefaction (Espinosa, 1976). Economic losses reached $1.1 billion (~$6.2 billion adjusted for inflation in 2025), equivalent to ~30% of Guatemala's gross domestic product at the time (Espinosa, 1976).

From a scientific point of view, the 1976 Motagua fault earthquake established several major tectonic facts in Central America. Before 1976, the Motagua fault's activity and regional importance remained poorly documented and understood (Molnar and Sykes, 1969; Muehlberger and Ritchie, 1975;

1. Department of Earth Sciences and Engineering, Missouri University of Science and Technology, Rolla, Missouri, U.S.A., https://orcid.org/0009-0006-4391-0938 (GC); https://orcid.org/0009-0005-4419-8244 (TM); https://orcid.org/0000-0002-3624-5961 (JM); https://orcid.org/0000-0001-7530-7128 (SSG); https://orcid.org/0000-0002-8734-3895 (JO-F); 2. Centro de Estudios Superiores de Energía y Minas (CESEM), Facultad de Ingeniería, Universidad de San Carlos de Guatemala, Guatemala City, Guatemala, https://orcid.org/0009-0009-2977-1638 (OGF); 3. Instituto Nacional de Sismología, Vulcanología, Meteorología e Hidrología, Guatemala City, Guatemala, https://orcid.org/0000-0002-5321-5377 (RY); 4. Department of Geosciences, University of Missouri-Kansas City, Kansas City, Missouri, U.S.A., https://orcid.org/0000-0002-6837-2594 (TN); 5. Institute for Geological Sciences, Friedrich-Schiller-University Jena, Jena, Germany, https://orcid.org/0000-0003-0777-2751 (CG); 6. Department of Geological Sciences, University of Missouri, Columbia, Missouri, U.S.A., https://orcid.org/0009-0007-0609-7180 (FG)

*Corresponding author: obristj@mst.edu

Cite this article as Clark, G., T. McEnaney, J. Maurer, A. Eckert, S. S. Gao, O. G. Flores, R. Yani, T. Niemi, C. Grützner, F. Gomez, *et al.* (2026). A Fiftieth Year Retrospective on the 1976 M_w 7.5 Motagua Earthquake in Guatemala, *Bull. Seismol. Soc. Am.* **XX**, 1–21, doi: 10.1785/0120250268

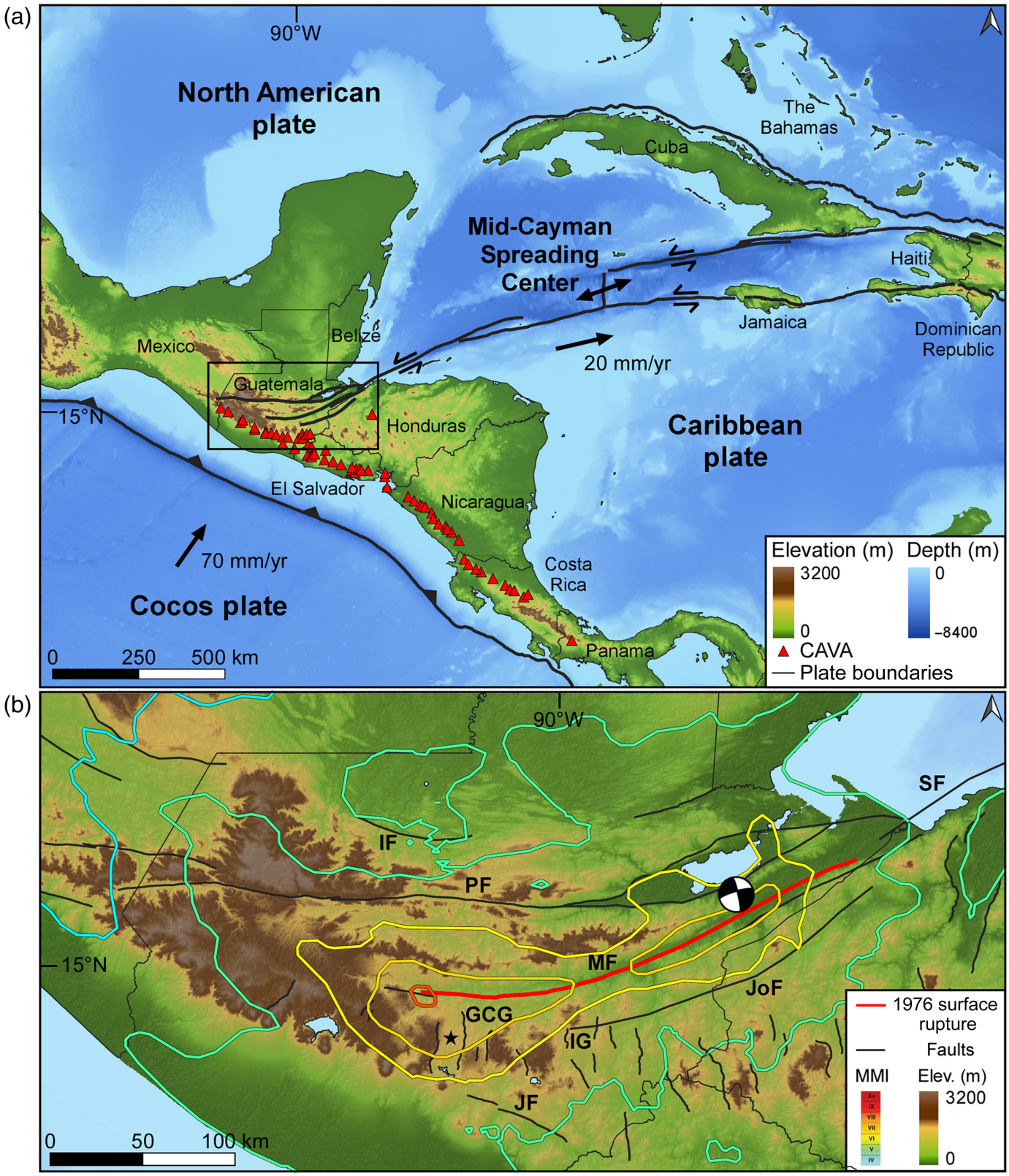

Figure 1. (a) Regional tectonic framework of the North American–Caribbean plate boundary. Red triangles show the location of volcanoes that make up the Central American volcanic arc (CAVA). Black box shows the outline of panel (b). (b) Modified Mercalli intensity (MMI) contours of the 1976 Motagua earthquake (from the U.S. Geological Survey [USGS] catalog; U.S. Geological Survey, 2025) and the rupture trace (red). The focal mechanism solution (FMS) shows the epicenter of the earthquake. Regional faults are shown in black and include the Ixcán fault (IF), Polochic fault (PF), Motagua fault (MF), Jalpatagua fault (JF), Guatemala City graben (GCG), Ipala graben (IG), Jocotán–Chamelecón fault (JOF), and Swan fault (SF; modified from the Global Earthquake Model (GEM) active fault database; Styron and Pagani, 2020). FMSs for the 1976 rupture from Kikuchi and Kanamori (1991). The location of Guatemala City is denoted as a black star. The color version of this figure is available only in the electronic edition.

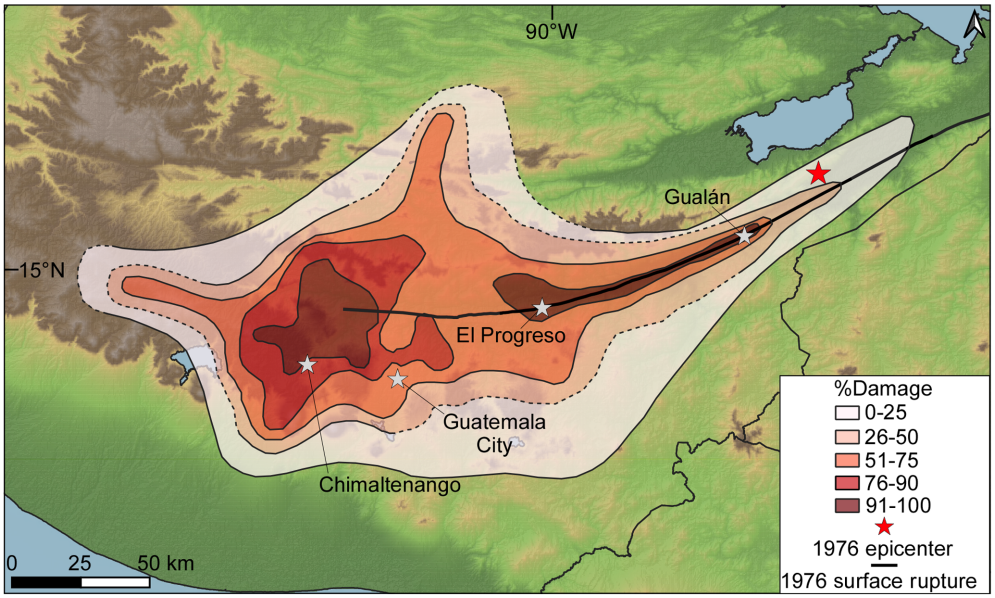

Figure 2. Contour map showing extent of adobe-type structures that collapsed during the 1976 event. Map modified from Espinosa *et al.* (1976). The color version of this figure is available only in the electronic edition.

compare with Schwartz, 1976). The earthquake, documented as a classic left-lateral strike-slip faulting event, served as proof that the Motagua fault is a major segment of the transform boundary between the North American and Caribbean plates in Guatemala. Following the event, the U.S. Geological Survey (USGS), in conjunction with the National Observatory (now the Guatemalan Institute for Seismology, Volcanology, Meteorology, and Hydrology), provided extensive documentation of the rupture and damage across the country (Espinosa, 1976; Matumoto and Latham 1976; Plafker *et al.*, 1976; Bucknam *et al.*, 1978; Seed *et al.*, 1981; Harp *et al.*, 1981). This allowed for a comprehensive analysis of one of the longest and largest documented strike-slip ruptures since the 1906 San Andreas earthquake (Plafker, 1976). Furthermore, the event offered a rare well-instrumented (for the time of the earthquake) example of a large intracontinental strike-slip earthquake and allowed seismologists to compare fault mechanics and rupture propagation, contributing to global models of strike-slip fault behavior. Field work validated surface ruptures with an average surface slip of 1.1 m (maximum of 3.4 m) and extensive afterslip and postseismic deformation processes (Bucknam *et al.*, 1978; Lisowski and Thatcher, 1981). Although the earthquake size and the surface rupture length were typical of large strike-slip earthquakes (Wells and Coppersmith, 1994; Thingbaijam *et al.*, 2017), the westward concentration of seismic energy release resulted in noteworthy damage distribution caused by rupture directionality (Fig. 2; Espinosa *et al.*, 1976). Subsequent seismic analysis indicated a complex, multisubevent rupture (Kanamori and Stewart, 1978; Kikuchi and Kanamori, 1982, 1991; Young *et al.*, 1989) and confirmed theoretical stress transfer predictions (Dewey and Julian, 1976; Langer and Bollinger, 1979).

In 2026, 50 yr after the earthquake, the Motagua fault, as part of the Polochic–Motagua fault system, has received limited research attention and compared with other major transform plate boundaries remains poorly monitored and understood. This review synthesizes five decades of research, summarizing the findings and implications of interseismic (including historic earthquake occurrence and the notable absence of a paleoseismic record), coseismic (including surface rupture characteristics, seismological source characteristics, evidence of rupture directivity, and environmental effects and ground-motion indicators), and postseismic (including aftershock, afterslip, and geodetic analyses) observations from the 1976 earthquake. This summary provides a basis for documenting how research on the 1976 Motagua earthquake advanced scientific understanding of the North American and Caribbean plate boundary and continental transform fault behavior in general. In addition, for the first time, we make legacy material available to the scientific community, including the digitization and preservation of analog field material using modern georeferencing techniques (McEnaney and Clark, 2025). It is our hope that these resources will spur continued research into this important event and the plate boundary as a whole.

THE POLOCHIC AND MOTAGUA FAULT SYSTEM

The Polochic–Motagua fault system forms the continental segment of the North American–Caribbean plate boundary in Guatemala, where ~18–20 mm/yr of left-lateral motion is accommodated between the two plates (DeMets *et al.*, 2000). The plate boundary extends from the Mid-Cayman Spreading Center through northern Guatemala to the Cocos–North America–Caribbean diffuse triple junction at the Guatemala City Graben (Fig. 1b; Authemayou *et al.*, 2011; Garnier *et al.*, 2022; Maurer *et al.*, 2025). The boundary transitions from a single-fault strand oceanic transform fault offshore to a more complex system of parallel and secondary strike-slip faults onshore, where deformation is partitioned across multiple structures rather than concentrated along a single trace (Guzmán-Speziale and Molina, 2022).

The oceanic segment of the plate boundary comprises the Mid-Cayman Spreading Center and the Swan fault, also referred to as Swan Islands fault. The Mid-Cayman Spreading Center is a spreading center accommodating 15–17 mm/yr of divergence

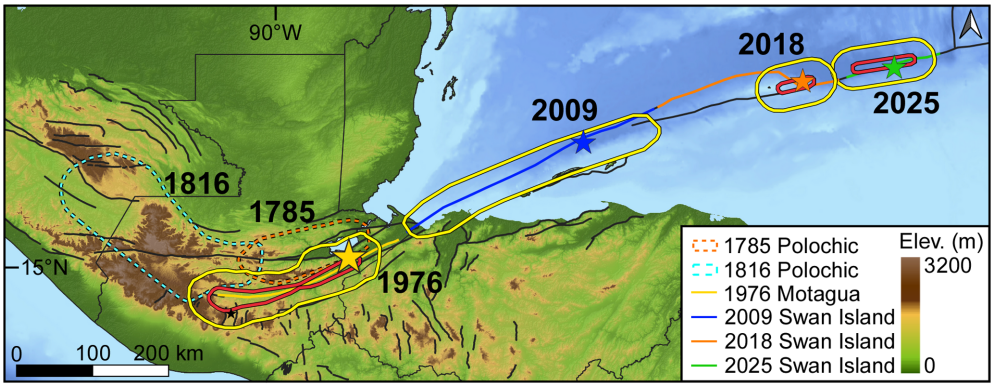

Figure 3. Major earthquakes (magnitude >7) since 1785 on the western segment of the North American–Caribbean plate boundary. Epicenters are shown with colored stars, and ruptured segments are shown in colored lines. Peak ground acceleration (PGA) contours showing 20%*g* (yellow) and 50%*g* (red; from USGS earthquake catalog; U.S. Geological Survey, 2025). The 1785 and 1816 Polochic earthquakes damage areas shown in orange and teal areas, respectively (White, 1984). Faults modified from the GEM active fault database (Styron and Pagani, 2020). The location of Guatemala City is denoted as a black star. The color version of this figure is available only in the electronic edition.

(Hayman *et al.*, 2011), and the Swan fault extends ~750 km westward from the southern end of the spreading center to Guatemala (Graham *et al.*, 2012). Recent ruptures on the Swan fault include the 2009 M_w 7.3 event (Graham *et al.*, 2012), the 2018 M_w 7.5 event (Cheng and Wang, 2020), and the 2025 M_w 7.6 event (Fig. 3; Kusky *et al.*, 2025). These events are notable because the 2009 and 2018 events were both supershear events and propagated mostly unilaterally from east to west (Bao *et al.*, 2022).

The Swan fault continues onshore as the Polochic–Motagua fault system in Guatemala. The Polochic–Motagua fault system consists of two principal left-lateral strike-slip faults that extend subparallel across Guatemala for ~350 km (Fig. 1b; Plafker *et al.*, 1976; Guzmán-Speziale and Molina, 2022). The Motagua fault traces along the Motagua River valley from the Caribbean coast westward to ~50 km north of Guatemala City (Schwartz *et al.*, 1979), accommodating the majority of plate boundary motion in eastern and central Guatemala (Lyon-Caen *et al.*, 2006; Franco *et al.*, 2012; Ellis *et al.*, 2019; Maurer *et al.*, 2025). The Polochic fault branches off the Motagua fault near the Caribbean coast of Guatemala and is separated from the Motagua fault by the Sierra de las Minas (Fig. 1b). The Polochic fault extends west into Chiapas, Mexico (White, 1984; Authemayou *et al.*, 2012). Both faults exhibit near vertical dips in the upper 15 km of the crust and do not appear to merge at depth (Franco *et al.*, 2009). The seismogenic zone extends to depths of 10–15 km, consistent with Global Positioning System (GPS)–derived locking depths of ~20 km for the Motagua fault and ~5 km for the Polochic fault (Franco *et al.*, 2009; Ellis *et al.*, 2019). Additional structures within the plate boundary zone include the Jocotán–Chamelecón fault system to the south and the Ixcán fault to the north (Fig. 1b), although the contemporary activity and slip rates on these structures remain poorly constrained (Schwartz *et al.*, 1979; Guzmán-Speziale and Molina, 2022). South of the Polochic–Motagua fault system, a series of north–south-trending structures accommodate distributed extension across the western end of the Caribbean plate. These include the Guatemala City graben, the Ipala graben, and the Chiquimula graben in Guatemala, as well as normal fault systems that extend into Honduras (Franco *et al.*, 2009; Rodriguez *et al.*, 2009; Ellis *et al.*, 2019).

Contemporary GPS measurements document the partitioning of plate boundary motion across the fault system (e.g., Franco *et al.*, 2012; Ellis *et al.*, 2019; Maurer *et al.*, 2025). The Motagua fault accommodates ~14.2 ± 1.6 mm/yr of left-lateral motion in eastern Guatemala at its junction with the Swan fault, representing ~80% of the total plate boundary motion (Lyon-Caen *et al.*, 2006; Franco *et al.*, 2012; Ellis *et al.*, 2019). Slip rates on the Motagua fault decrease systematically westward to the Guatemala City graben, with rates falling below 2 mm/yr west of the graben (Ellis *et al.*, 2019). This westward decrease reflects the transfer of motion southward into the extensional zone between the Motagua fault and the Central American volcanic arc (CAVA; Fig. 1a; Rodriguez *et al.*, 2009; Ellis *et al.*, 2019). The Polochic fault accommodates the remaining ~20% of the total plate boundary motion (Franco *et al.*, 2012; Ellis *et al.*, 2019). The partitioning of motion between these two faults represents a significant change from conditions during the Miocene, when the Polochic fault was the dominant structure (Bartole *et al.*, 2019; Obrist-Farner *et al.*, 2020). This transition from Polochic fault dominance to the current Motagua fault-dominated configuration occurred over approximately the past seven million years (Obrist-Farner *et al.*, 2020).

THE 1976 MOTAGUA EARTHQUAKE

Legacy data from the 1976 event

Although the 1976 earthquake was well documented, material related to the earthquake was archived in analog formats, limiting accessibility to the scientific community. We present digitized rupture measurements from systematic field mapping (Fig. 4), original topographic maps with field annotations during USGS surveys, and a georeferenced collection of 1:10,000 scale aerial photographs spanning the western and central segments of the surface rupture (McEnaney and Clark, 2025). This

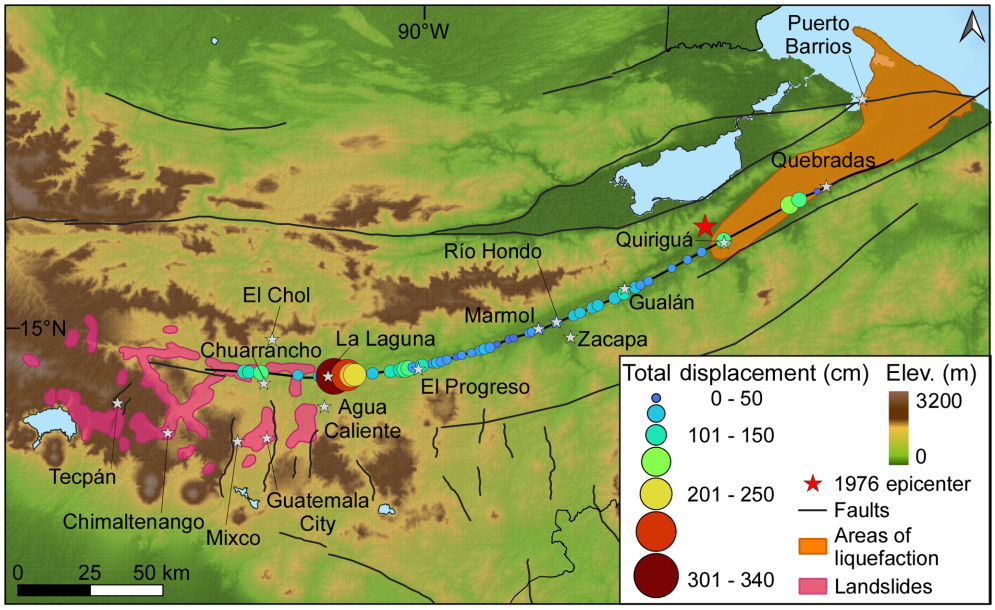

Figure 4. Total displacement measurements taken in April 1976 (Bucknam *et al.*, 1978) along the surface rupture trace. Also shown are landslides (pink regions) and areas of extensive liquefaction (orange region) caused by the 1976 earthquake (Plafker *et al.*, 1976). Faults modified from the GEM active fault database (Styron and Pagani, 2020). White stars show locations of cities and towns discussed in the text. The color version of this figure is available only in the electronic edition.

archive also includes an extensive collection of 35 mm color photographs taken by the USGS team during the expedition (Fig. 5), many of which have not been previously published. We include digitized field notebooks containing detailed observations, measurements, and sketches along with previously published aftershock datasets (Person *et al.*, 1976; Langer and Bollinger, 1979; White and Harlow, 1979) converted to standardized digital formats (McEnaney and Clark, 2025).

Coseismic observations

Surface rupture and field observations. The 1976 Motagua earthquake produced ~240 km of surface rupture along the fault, extending from the lower Motagua Valley in eastern Guatemala to ~50 km north of Guatemala City in the west (Fig. 1b; Plafker *et al.*, 1976). This rupture extended the previously recognized western limit of the fault by 85 km. To the east of the epicenter, the surface trace could not be confirmed because of thick vegetation cover, introducing uncertainty in the precise eastern extent of surface breakage.

Surface displacement along the trace was dominantly left lateral with an average offset of 1.1 m over the entire rupture length (Fig. 4; Plafker *et al.*, 1976). Maximum-horizontal displacement reached 3.40 m ~40 km from the western termination of the earthquake rupture (Fig. 4). Field measurements documented systematic spatial variations in displacement magnitude along the rupture, with regions of above-average slip corresponding to areas of concentrated moment release identified in seismological analyses (Young *et al.*, 1989). Vertical offsets were generally minor relative to horizontal displacement, varying spatially along the rupture (Plafker *et al.*, 1976). Most locations showed vertical components <30% of horizontal offset, with down-to-the-north or down-to-the-south motion depending on local fault geometry. A notable exception occurred along a 10 km segment near the easternmost mapped extent of the surface trace, where vertical displacement was consistently down to the north and locally reached 50% of the sinistral component.

The surface expression of the fault zone exhibited considerable complexity (Fig. 5), with individual fractures reaching lengths of ≤10 m with variable amounts of dilation ≤10 cm. En echelon fractures were oriented at angles ≤35° to the main fault trace, reflecting the distributed nature of deformation within the shallow fault zone. The fault zone width varied from 1 to 9 m, with maximum-observed widths of ~9 m at localities where the fault surface was exposed in highway cuts. Field documentation of these features, including distinctive mole tracks and large lateral offsets, provided detailed characterization of surface rupture morphology (Fig. 5).

Secondary faulting occurred concurrent with the main rupture, with connected faults relatively scarce along most of the rupture length. Notable occurrences included areas near El Progreso, where a subsidiary fault ~1 km long with 20 cm sinistral displacement was oriented roughly parallel to the main fault trace, and near Chuarrancho, where a prominent surface break splayed off the main trace in a northeasterly direction with a sinistral offset of 28 cm (Fig. 4; Plafker *et al.*, 1976). Additional secondary fault systems concentrated primarily south and southwest of the western Motagua fault terminus extended as far as 30 km from the main fault trace but did not connect to the primary rupture at the surface. Individual secondary faults ranged in length from ~100 m to 3.5 km, with strikes commonly between N10°E and N30°E (Plafker *et al.*, 1976). These secondary structures included reactivated faults and pre-existing features within the Guatemala City graben system, causing substantial damage to houses, roads, and infrastructure in Guatemala City.

Figure 5. Field photographs showing different characteristics of the surface rupture. (a) Fault trace at La Laguna looking west. (b) Maximum-observed displacement at La Laguna (340 cm) offsetting a stone fence. (c) En echelon cracks along the fault trace near El Chol. (d) A toppled Ceiba tree near Quebradas, with the surface rupture passing directly below it. Person for scale highlighted with red arrow. (e) Offset road and drainage ditch in Hwy CA-10 near Rio Hondo. All locations discussed in the photos are shown in Figure 3. Photos taken by the USGS in 1976. The color version of this figure is available only in the electronic edition.

Seismological source characterization. Recordings from the World-Wide Standard Seismograph Network provided long-period surface and body waves for source characterization. *P*-wave first-motion data and Love-wave analysis established left-lateral strike-slip faulting along a near-vertical plane with strike varying from N66°E to N98°E, consistent with the Motagua fault geometry at the epicenter (Fig. 1b; Dewey and Julian, 1976; Kanamori and Stewart, 1978).

Source inversion models documented significant spatial and temporal complexity in the rupture process with significant model uncertainties. The earthquake models suggest an asymmetric, segmented, bilateral rupture along the curved Motagua fault system, made of 5–10 subevents, with total seismic moments varying between 2.1 and 3.7×10^{20} N · m (Fig. 6; Kanamori and Stewart, 1978; Kikuchi and Kanamori, 1982; Young *et al.*, 1989). Although the M_w 7.5 magnitude has been persistently used, the range of moment released corresponds to an M_w 7.5–7.7 earthquake.

Surface-wave directivity analysis indicated an asymmetric bilateral faulting pattern with ∼70% of moment release propagating westward, optimally modeled with eastern and western segments of 75 and 175 km, respectively (Kanamori and Stewart, 1978). Early analyses using European-only arrays were unable to distinguish bilateral from unilateral rupture (Kikuchi and Kanamori, 1982). Later analyses incorporating 17 stations with better azimuthal coverage established true asymmetric bilateral propagation, though substantial errors indicated significant unresolved complexity (Young *et al.*, 1989).

Rupture velocity estimates range from 2.0 to 3.5 km/s, though this parameter is poorly constrained by teleseismic data. Surface-wave modeling used values of 2.5–3.0 km/s resolving directivity patterns (Kanamori and Stewart, 1978). Body-wave inversions either assumed rupture velocities as input constraints (Kikuchi and Kanamori, 1991) or calculated approximate values from inferred timing and spacing of moment release episodes (Kikuchi and Kanamori, 1982; Young *et al.*, 1989). The inherent nonuniqueness means multiple combinations of rupture velocity, subevent locations, and moment distributions can explain observations equally well (Kikuchi and Kanamori, 1991).

The largest individual moment release subevents varied substantially between studies ($5.3–9 \times 10^{19}$ N · m) but consistently occurred ∼90 km west of the epicenter at ∼22–72 s after rupture initiation (Fig. 6b; Kanamori and Stewart, 1978; Kikuchi and Kanamori, 1982; Young *et al.*, 1989), coinciding with maximum surface displacement observations. More than 60% of total moment occurred between 60 and 120 km west of the epicenter, indicating heterogeneous mechanical properties controlled by asperities or varying frictional characteristics.

Dip-slip motion contributed disproportionately to modeled surface-wave amplitudes despite comprising only ∼10% percent of total scalar moment (Kikuchi and Kanamori, 1991). Normal faulting near the epicenter (1.5×10^{19} N · m) and reverse faulting at the western terminus (1.1×10^{19} N · m) were identified, with these dip-slip components contributing *P*- and *PP*-wave amplitudes comparable to much larger strike-slip events. The reverse faulting component at the western terminus contrasted with field observations documenting predominantly normal faulting (Plafker *et al.*, 1976; Langer and Bollinger, 1979), highlighting fundamental nonuniqueness in teleseismic inversions.

Average stress-drop estimates were ∼30 bars, comparable to worldwide averages for interplate earthquakes (Kanamori and Stewart, 1978). Assuming a seismogenic width of 15 km, seismological analysis indicated average displacement of ∼2 m. A discrepancy emerged between this seismologically inferred displacement and the initially measured surface offset averaging 1.1 m (Plafker *et al.*, 1976), possibly reflecting depth-dependent deformation, off-fault deformation, surface layer decoupling, and postseismic creep subsequently documented through field remeasurement campaigns (Bucknam *et al.*, 1978).

Paleoseismic evidence for rupture directivity. Recent analysis of sediment records from six Guatemalan lakes has provided independent evidence for directivity effects during the 1976 earthquake, offering additional constraints on the spatial distribution of ground motion beyond instrumental observations (Fig. 7; Obrist-Farner *et al.*, 2025). Deposits from turbidites triggered by the earthquake were identified in five lakes, with their thickness distribution reflecting the asymmetric nature of shaking during the rupture. Lake Atitlán, located ∼40 km southwest of the western rupture terminus, contained the thickest event deposits despite being the most distant from the earthquake epicenter. Lakes positioned closer to the epicenter but perpendicular to the primary rupture propagation path contained substantially thinner deposits. Lake Izabal, located near the epicenter but north of the fault trace, showed no detectable event deposit despite fractures extending to the lake floor that suggest sensitivity to seismic activity (Obrist-Farner *et al.*, 2023). Although factors such as site response, sedimentation rate, and sediment composition can influence the resulting thickness of event deposits, the spatial pattern supports seismological evidence for strong westward directivity (Obrist-Farner *et al.*, 2025), for which >70% of moment release occurred west of the epicenter (Kanamori and Stewart, 1978).

The sediment record also aligns with instrumental observations of asymmetric bilateral rupture (Young *et al.*, 1989) and enhanced ground-motion concentration near the western fault terminus, where the largest individual moment release episodes occurred ∼90 km west of the epicenter (Fig. 6; Kikuchi and Kanamori, 1982; Young *et al.*, 1989). The correlation between thick lake deposits at Lake Atitlán, concentrated landslide activity west of Guatemala City (Fig. 4; Harp *et al.*, 1981), and quasi-dynamic rupture modeling results provides evidence that directivity controlled the spatial distribution of strong ground motion (Fig. 7; Obrist-Farner *et al.*, 2025).

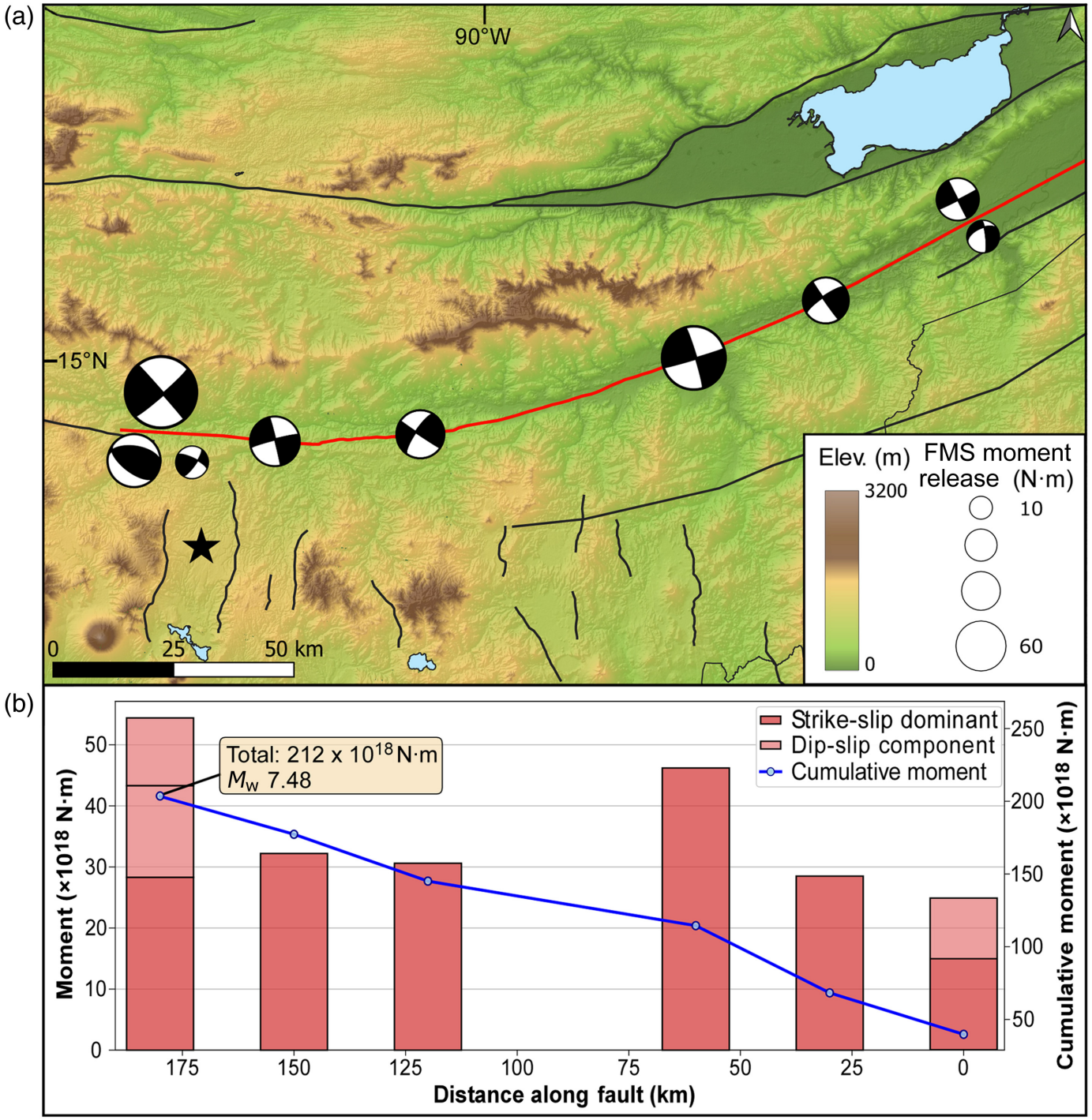

Figure 6. (a) The 1976 Motagua fault surface rupture (red) with the FMS of the modeled subevents from Kikuchi and Kanamori (1991), scaled proportionally to seismic moment. Black lines show major faults from the GEM global active faults database (Styron and Pagani, 2020). The location of Guatemala City is denoted with a black star. (b) Moment estimates for the modeled subevents from Kikuchi and Kanamori (1991). The color version of this figure is available only in the electronic edition.

Ground failures. Comprehensive landslide mapping using high-altitude U-2 aerial photography provided systematic documentation of earthquake-induced slope failures across the affected region (Harp *et al.*, 1981). The earthquake generated >10,000 landslides across ~16,000 km^2, causing hundreds of fatalities and severely disrupting transportation networks (Fig. 4). The predominant types were rock falls and debris slides, most <15,000 m^3 in volume, with 11 events >100,000 m^3. Rock falls typically occurred on slopes steeper than 50° as tensile failures from seismic-wave reflection off

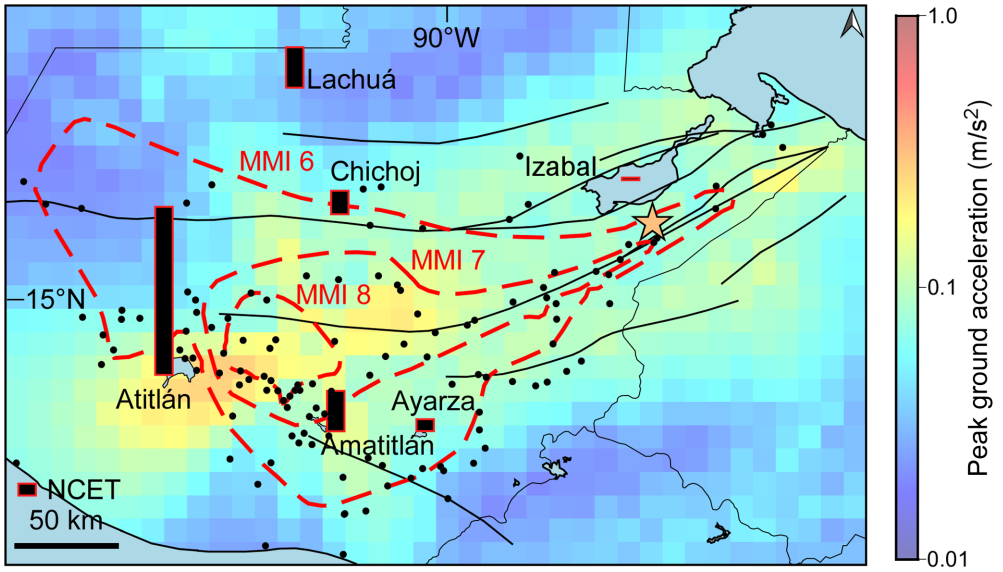

Figure 7. Modeled PGA values from the quasi-dynamic rupture model modified from Obrist-Farner *et al.* (2025). Black bars are normalized cumulative event thickness (NCET) from the studied lakes. Red contours are MMI contours showing areas of damage and black dots are locations with completed MMI questionnaires (Espinosa *et al.*, 1976). NCET at Lake Izabal is zero. The color version of this figure is available only in the electronic edition.

canyon walls. Debris slides developed on gentler slopes (30°–50°) in thin, noncohesive soil layers overlying Pleistocene pumice deposits. Approximately 90% of landslides occurred within Pleistocene pumice deposits, which cover only ~20% of the affected region. The highest density of landslides occurred in the highlands west of Guatemala City.

Extensive liquefaction occurred south of Guatemala City near Lake Amatitlán, in the Motagua Valley, along the Atlantic coast of Guatemala and Honduras, near Lake Atitlán to the west of Guatemala City, and along Lake Ilopango in El Salvador (Fig. 4; Plafker *et al.*, 1976). Effects included lateral spreading extending ≤1 km from the main rupture, ground settlement reaching 1 m, and ground cracks >100 cm in width (Caccavale *et al.*, 2019). The affected soils consisted of pumiceous sand layers with relatively low density, making them particularly vulnerable to earthquake-induced liquefaction (Seed *et al.*, 1981).

Postseismic observations

Aftershock sequence. Three seismograph networks documented the aftershock sequence following the 4 February mainshock. A six-station permanent array with vertical seismometers distributed across an area with an approximate diameter of 140 km west of Guatemala City maintained continuous monitoring through 30 June 1976 (Fig. 8a; White and Harlow, 1979). The USGS deployed portable networks in two sequential campaigns, one in the western part of the rupture (eight stations) and one in the eastern part of the rupture with 10 stations (Fig. 8a; Langer *et al.*, 1976; Langer and Bollinger, 1979). An additional temporary deployment of two portable stations operated at six sites between 6 and 10 February, supplemented by a station at Tegucigalpa, Honduras (Matumoto and Latham, 1976).

The permanent network captured secondary faulting south of the western Motagua fault terminus. During the 11 months preceding the earthquake, background seismicity averaged less than one event per day. The mainshock triggered a >50-fold increase in seismicity rates (White and Harlow, 1979). Events were initially timed only for days bracketing nine major aftershocks with body-wave magnitude >4.2 through March 1976. Processing of all events with magnitude >1.5 resumed after 1 April (White and Harlow, 1979). The permanent network catalog provides hypocentral data for 1560 events between 1 February and 30 June 1976 (White and Harlow, 1979). Data demonstrated extensive fracturing between the western Motagua fault and the volcanic chain (Fig. 1), with diffuse seismicity and normal fault mechanisms (White and Harlow, 1979).

A temporary two-station deployment during the first week following the mainshock captured intense initial aftershock activity and revealed patterns of fault activation. Matumoto and Latham (1976) recorded several thousand earthquakes between 6 and 10 February 1976, with adjusted daily counts reaching ≤~5000 events per day at individual sites. The temporal decay of these single-station aftershock rates showed a decline consistent with the classical formulation of Omori's law (Utsu, 1961), although no formal modified Omori-law parameter inversion was performed. Owing to the limited two-station geometry and short recording intervals, only events recorded simultaneously at multiple stations could be reliably located with this subset being composed of 95 aftershocks. These were used to delineate the spatial extent of postmainshock fault activation, which was defined by a seismically active zone that initially followed the Motagua fault before branching sharply southward ~35 km west of Guatemala City. The highest aftershock activity during the observation period was concentrated along the western extremity of the rupture.

Subsequent USGS portable networks constrained the spatial extent of aftershock activity and documented systematic patterns in epicenter distribution. The western network operated from 9 to 17 February 1976, and the eastern network operated

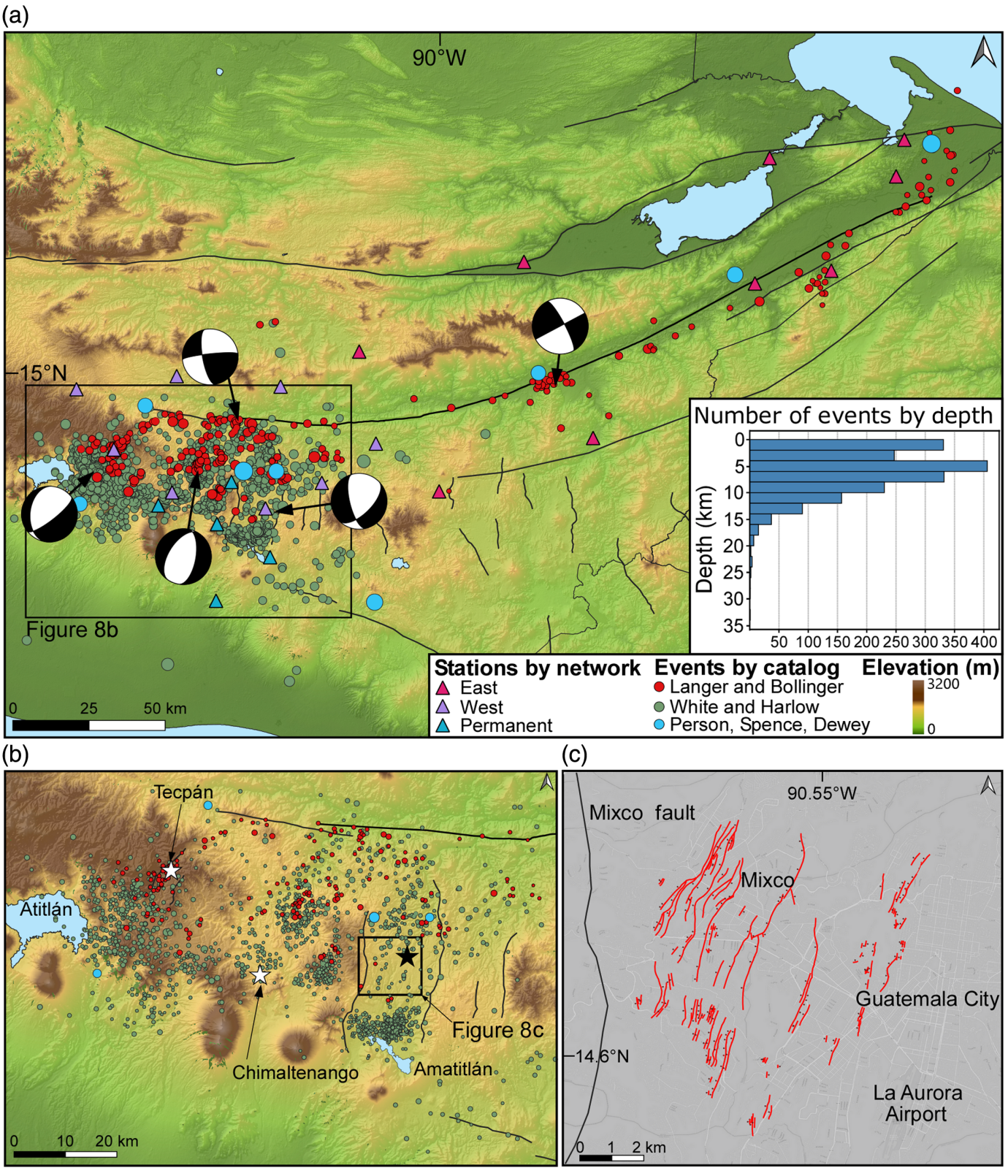

Figure 8. (a) Spatial distribution of aftershocks from the 1976 Motagua earthquake. Teleseismically detected events are shown in blue (Person *et al.*, 1976), events detected by the temporary network are shown in red (Langer and Bollinger, 1979), and events detected by the permanent network stations are shown in green (White and Harlow, 1979). Composite focal mechanisms are displayed for selected aftershocks (Langer and Bollinger, 1979). Faults modified from the GEM Active Fault Database (Styron and Pagani, 2020). Black box shows the outline of panel (b). Inset shows number of events per depth interval using the combined aftershock catalogs. (b) Same as A but focused on the western end of the rupture. Location of Guatemala City denoted as a black star. Black box shows the outline of panel (c). (c) Secondary faulting (red lines) mapped by the USGS in the Guatemala City Graben. The color version of this figure is available only in the electronic edition.

from 18 to 27 February 1976 (Fig. 8; Langer *et al.*, 1976; Langer and Bollinger, 1979). The investigation located 78 hypocenters with magnitude thresholds of ∼2.2, later expanded by 178 aftershocks for a combined total of 256 hypocenters (Langer *et al.*, 1976; Langer and Bollinger, 1979). Aftershock epicenters extended ∼300 km from the Gulf of Honduras westward to the Guatemalan highlands northeast of Lake Atitlán (Fig. 8a; Langer *et al.*, 1976). At the eastern extent, 12 epicenters were documented southeast of Puerto Barrios, with 8 aftershocks aligned with the inferred Motagua fault extension. Langer *et al.* (1976) interpreted this as the eastern rupture terminus, though these could alternatively represent stress-triggered seismicity on adjacent structures. The seismic moment release from aftershocks was generally uniform along the rupture trace but with notable concentration west of Zacapa corresponding to areas of above-average surface slip (Fig. 4; Langer *et al.*, 1976). Aftershock patterns exhibited systematic 2–3 km southerly offsets, suggesting steep south dip of the fault plane or significant velocity contrasts across the fault zone (Langer *et al.*, 1976).

Aftershocks revealed a linearized pattern extending ∼50 km beyond the main fault surface breakage (Fig. 8; Langer and Bollinger, 1979). At the western Motagua fault terminus, epicenters splayed southwest along surface lineaments, with concentration toward the Mixco-Guatemala City region (Langer and Bollinger, 1979). Both networks documented extensive seismicity on secondary faults south of the Motagua fault and west of longitude 90.3° W, with focal depths from near-surface to ∼14 km (Langer *et al.*, 1976; Langer and Bollinger, 1979; White and Harlow, 1979). Most aftershocks west of longitude 90.3° W were associated with secondary faulting in the Tecpán, Chimaltenango, Guatemala City, and Agua Caliente regions (Fig. 4; Langer *et al.*, 1976). Matumoto and Latham (1976) inferred a total rupture length of at least 250 km based on the spatial extent of aftershock activity.

Focal mechanism solutions revealed east-northeast–west-southwest left-lateral strike-slip faulting along the Motagua fault and northeast–southwest normal faulting on western terminus splays (Fig. 8a; Langer and Bollinger, 1979). The Mixco fault zone experienced normal dip-slip motion during the mainshock and a large aftershock on 6 February with body-wave magnitude 5.8 (Langer and Bollinger, 1979). The two largest aftershocks, both M_b 5.8, were normal events on the Mixco fault near Guatemala City (Person *et al.*, 1976; Langer and Bollinger, 1979). This secondary normal faulting correlated with theoretical stress patterns at strike-slip fault termini (Langer and Bollinger, 1979).

Afterslip observations. Field measurements documented extensive afterslip along the Motagua fault surface rupture through systematic remeasurement campaigns at eight sites distributed along the fault trace (Bucknam *et al.*, 1978). Three sites within a 50 km segment were regularly revisited over the following 2 yr. The monitoring used direct measurements of offset cultural features, including fence lines, building foundations, and roads, with measurement uncertainties of ∼1 cm (Bucknam *et al.*, 1978). No instruments were installed to record afterslip directly. Measurements were made using noninstrumental methods such as visual alignment of offset features, with a standard deviation of ≤1 cm, meaning that smaller amounts of afterslip were near the measurement limit (Bucknam *et al.*, 1978). Initial field surveys in April 1976 established baseline displacements that averaged 1.1 m across the monitored fault section (Bucknam *et al.*, 1978). Subsequent remeasurements revealed continued displacement accumulation, with temporal evolution characterized by both gradual slip and episodic behavior (Bucknam *et al.*, 1978).

The three sites with complete time histories demonstrated the range of afterslip behavior across the monitored section (Fig. 4). At Gualán, displacement increased from 0.93 m four days after the earthquake to 1.06 m by 1745 days, representing 0.13 m of afterslip. At Zacapa, displacement increased from 0.6 m on 8 February 1976 to 0.91 m by 1565 days, representing 0.31 m of afterslip. At Marmol, initial measurements were complicated by temporary concrete repairs installed after the earthquake, but subsequent monitoring documented continued afterslip accumulation to 0.20 m by ∼4 yr after the earthquake (Bucknam *et al.*, 1978). The afterslip magnitude at Zacapa represented approximately one-third of the initial coseismic displacement at that location. Episodic behavior was observed at several monitoring sites, including a steplike increase of 1.1 cm recorded during a small aftershock, though this displacement surge did not propagate to another monitoring site positioned 10 km along strike, indicating spatial variability in afterslip coupling and response to seismic triggering. Some short-term temporal variations in afterslip rate suggested possible displacement surges or episodic activity. Temporal correlation between elevated afterslip rates and increased aftershock activity suggested mechanical interaction between continued fault displacement and stress redistribution within the fault zone (Bucknam *et al.*, 1978).

Afterslip time histories demonstrated that displacement was proportional to the logarithm of time since the earthquake, with initial rates of several millimeters per day during the first weeks following the mainshock that decayed progressively over subsequent months (Bucknam *et al.*, 1978). An inverse relationship emerged between total coseismic displacement and subsequent afterslip rate across the monitored sites (Bucknam *et al.*, 1978). Locations that experienced the largest coseismic displacement were associated with the lowest rates of afterslip, and locations with smaller coseismic displacement corresponded to the highest afterslip rates (Bucknam *et al.*, 1978). This spatial pattern extended along the ∼50 km monitored section and indicated heterogeneous frictional properties along the fault surface, with areas of high coseismic slip representing zones of more complete stress release during

the mainshock and areas of lower coseismic slip accommodating proportionally more postseismic deformation (Bucknam *et al.*, 1978).

By 1980, slip rates at the three comprehensively monitored sites had converged to ~23 mm per year, exceeding not only current estimates for the Motagua fault specifically but also estimates of overall plate boundary motion between the North American and Caribbean plates (Lisowski and Thatcher, 1981; DeMets *et al.*, 2000; Franco *et al.*, 2012; Ellis *et al.*, 2019; Maurer *et al.*, 2025). These anomalously high-postseismic rates indicate that the 1976 earthquake did not completely release accumulated strain, with continued displacement representing the release of residual elastic strain following incomplete coseismic rupture. Understanding the mechanism of this sustained postseismic deformation requires examining the depth and character of the deformation zone. The regular spatial variation in total slip and afterslip along ~50 km of the fault trace suggested that afterslip was not controlled by local near-surface geological factors such as alluvial cover (Bucknam *et al.*, 1978). Studies of afterslip following the 1966 Parkfield earthquake in California indicated a significant component caused by thick alluvium ranging from 0.5 to 3 km in thickness (Scholz *et al.*, 1969), but in Guatemala, the poorly consolidated Quaternary alluvium was estimated to be <100 m thick, too thin to explain the observed afterslip magnitudes and patterns (Bucknam *et al.*, 1978). Instead, the fault-scale spatial coherence of afterslip behavior supported a mechanism involving stable frictional sliding within a mechanically distinct layer several kilometers thick, comparable to the ~4-km-thick layer proposed for the Parkfield segment of the San Andreas fault (Scholz *et al.*, 1969; Bucknam *et al.*, 1978). Within this deeper crustal layer, frictional properties permit continued time-dependent displacement as residual strain from the incomplete mainshock rupture is progressively released through stable sliding rather than seismic failure (Bucknam *et al.*, 1978).

Geodetic observations. A 15-station geodetic network extending 10 km north and 40 km south of the fault, surveyed in 1935 and 1953, was reobserved in 1978 (Lisowski and Thatcher, 1981). The 1978 survey used electronic distance measurement with standard errors of ~10 mm (Lisowski and Thatcher, 1981).

Analysis of 45 common angles revealed systematic horizontal deformation concentrated in the fault-crossing section (Lisowski and Thatcher, 1981). The fault-crossing subsection exhibited accumulated shear strain of 49 ± 5 μstrain with the azimuth of maximum left-lateral shear oriented N54°E ± 4°, closely matching the N65°E strike of the Motagua fault (Lisowski and Thatcher, 1981), consistent with expected displacement gradient for left-lateral slip on the fault.

Dislocation modeling using elastic half-space theory converted observed angle changes into fault-slip estimates (Lisowski and Thatcher, 1981). A uniform-slip model extending from 0 to 15 km depth yielded left-lateral slip of 1.3 ± 0.1 m (Lisowski and Thatcher, 1981). A three-segment model allowing slip to vary with depth indicated 0.8 ± 0.1 m near the surface, increasing to 2.1 ± 0.5 m at 5–15 km depth, with slip below 15 km poorly constrained at 0.8 ± 1.2 m (Lisowski and Thatcher, 1981). The multisegment model provided superior fit and better agreement with the ~2 m of slip inferred from seismic moment calculations (Kanamori and Stewart, 1978), suggesting depth-dependent slip distribution with maximum displacement at seismogenic depths.

KNOWLEDGE GAINED SINCE THE 1976 EARTHQUAKE

Slip rates on the plate boundary and individual fault strands

Slip rates on the main faults of the Polochic–Motagua fault system based on field observations are scarce. Progressive offset of stream terraces at the Rio El Tambor–Rio Motagua confluence near Zacapa documents recurrent left-lateral displacement on the Motagua fault, with the youngest mappable terrace displaying 23.7 m offset and the oldest 58.3 m (Fig. 9; Schwartz *et al.*, 1979). Age constraints based on volcanic tuff and soil development indicate the oldest terrace is younger than 40,000 yr and older than 10,000 yr, yielding late Quaternary slip rates of 1.5–6 mm/yr (Schwartz *et al.*, 1979). Similar geomorphic evidence along the Polochic fault, including offset streams of 35–100 m, suggests comparable Quaternary activity (Schwartz *et al.*, 1979). Schwartz *et al.* (1979) estimated combined the late Quaternary slip rate at 4.5–18 mm/yr for the plate boundary. South-facing scarps along both faults indicate an up-to-the-north vertical component representing up to 5% of lateral slip (Schwartz *et al.*, 1979).

Contemporary GPS-based estimates suggest substantially higher slip rates on the Motagua fault (Franco *et al.*, 2012; Ellis *et al.*, 2019). These studies, however, used relatively simple block models that did not account for distributed deformation, leading to discrepancies between geodetic and geologic slip rates. Recent advances have refined slip-rate estimates and suggest distributed contemporary deformation. Maurer *et al.* (2025) used multiple complementary methods, including strain-rate calculations, 3D elastic dislocation modeling, and 2D finite-element modeling, demonstrating that minor fault segments including the Ixcán fault and Jocotán–Chamelecón fault zone (Fig. 1b) are active and accommodate some proportion of total plate rate. Inclusion of these minor strands and allowing for inelastic bulk crustal strain resolves some discrepancies, with overall lower Motagua fault slip rates (~6 to 8 mm/yr) in closer agreement with geological rates (Maurer *et al.*, 2025). For the Polochic fault, estimated slip rates are slightly higher than the geologic rates (~3 to 7 mm/yr varying along strike), with minor fault segments accommodating 1–3 mm/yr (Maurer *et al.*, 2025).

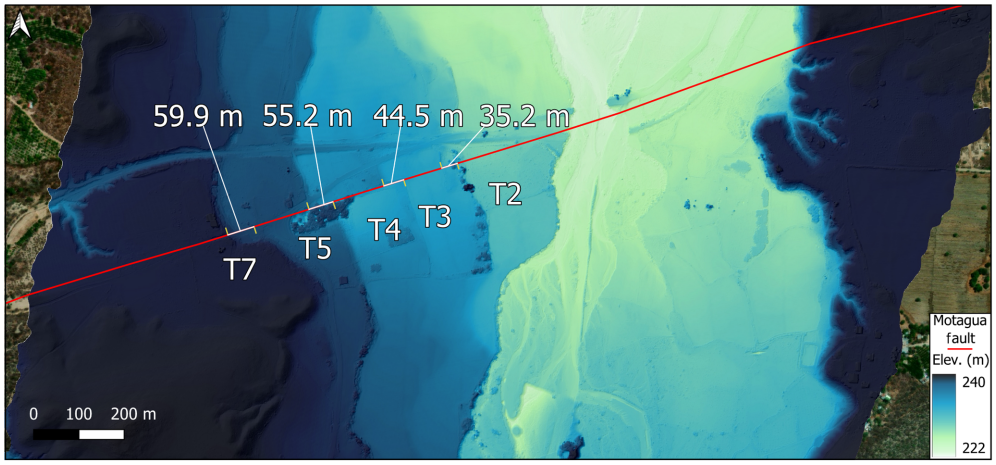

Figure 9. High-resolution drone light detection and ranging (lidar) imagery acquired in 2024 showing the El Tambor River terraces originally documented by Schwartz *et al.* (1979). Terrace surfaces T7, T5, T4, T3, and T2 are labeled following their original classification. Modern agricultural and infrastructural modification between T4–T3 and T3–T2 boundaries resulted in uncertainty in terrace-offset estimates and should be considered when interpreting displacement magnitudes. The color version of this figure is available only in the electronic edition.

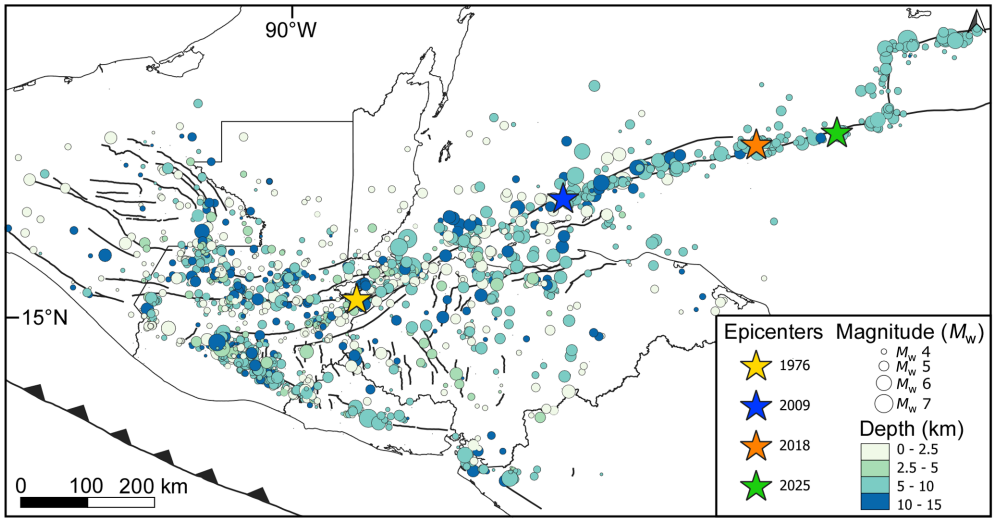

Figure 10. Spatial distribution of upper-crustal (depths ≤15 km) seismic events (magnitude M_w>4) in Central America since 1977. Major rupture epicenters are shown with a star. Events are scaled by magnitude and colored by size. The catalog was compiled from the USGS earthquake catalog (U.S. Geological Survey, 2025) and the catalog provided by Gamboa-Cante *et al.* (2024). All events associated to the subduction zone have been removed. Faults modified from the GEM active fault database (Styron and Pagani, 2020). The color version of this figure is available only in the electronic edition.

An extensional zone in the Caribbean plate south of the plate boundary also accommodates distributed deformation between the Motagua fault and the CAVA (Fig. 1a), accommodating 3–5 mm/yr of east–west extension, approximately one-quarter of the total left-lateral plate-boundary motion. Extension is accommodated through normal and oblique-normal faults defining the Guatemala City and Ipala grabens and by dextral motion along the Jalpatagua–Santa Rosa fault system (Fig. 1b; Garnier *et al.*, 2021). These structures define the southern expression of distributed strain transfer from the Polochic–Motagua fault system into the western Caribbean fore-arc (Garnier *et al.*, 2022).

Seismicity on the plate boundary

Permanent seismic network coverage of the Polochic–Motagua fault system has remained sparse since 1976. A six-month deployment of 30 seismic stations in 2005 provided the most comprehensive characterization of microseismicity patterns along the eastern segment of the fault system (Franco *et al.*, 2009). This network recorded 502 local events, with 276 earthquakes precisely located using at least four station observations.

The deployment revealed active seismicity concentrated in the upper 15 km of crust, with the seismogenic zone extending to 10–15 km depth beneath both the Polochic and Motagua faults. This depth range corresponds closely to the ~20 km locking depth derived from GPS models of strain accumulation on the Motagua fault (Lyon-Caen *et al.*, 2006; Franco *et al.*, 2012), confirming the thickness of the mechanically coupled zone. Microseismic activity occurred at comparable rates on both principal faults, distributed along fault traces rather than concentrated in specific segments. Earthquake clusters within north–south-trending grabens south of the Motagua fault exhibited normal faulting on westward-dipping planes, whereas clusters within fold structures north of the Polochic fault showed reverse faulting on south-dipping planes. These focal mechanisms match the GPS-observed transition from dominant east–west strike-slip motion to dominant east–west extension, confirming secondary structures actively participate in accommodating plate boundary deformation.

The comparable microseismic activity on both faults presents an apparent contradiction with geodetic observations. GPS measurements show the Motagua fault accommodates the majority of elastic strike-slip deformation while minimal strain accumulates across the Polochic fault (Franco *et al.*, 2012; Ellis *et al.*, 2019; Maurer *et al.*, 2025). Yet the six-month deployment documented similar earthquake activity rates on both structures. This discrepancy suggests that short-term seismicity patterns may not directly reflect long-term strain accumulation, potentially indicating temporal variations in fault activity, episodic behavior, or substantial aseismic strain release on the Polochic fault.

Regional catalogs confirm seismic activity extends across multiple structures beyond the two principal faults, including the Ixcán, Jocotán–Chamelecón, and other associated fault segments, as well as distributed activity within graben systems (Fig. 10; Guzmán-Speziale and Molina, 2022). This broad distribution further supports geodetic evidence for strain accommodation across a wide plate boundary zone.

Instrumentation limitations influence interpretation of seismicity along the plate boundary. The permanent network maintained since 1976 has poor location control, characterized by high azimuthal gap angles >180° and distances to nearest stations >50 km (González-Negreros and Gaspar-Escribano, 2025). The recent strengthening of the Guatemala National Seismological Network (Yani-Quiyuch *et al.*, 2023) is generating higher-quality data, although completeness magnitude averages around **M** 4.0 for shallow earthquakes along the Polochic–Motagua fault system compared with **M** ≤3.0 in better-monitored areas (Gamboa-Canté *et al.*, 2024). The velocity model has remained unchanged since 1980, potentially contributing to systematic location uncertainties (González-Negreros and Gaspar-Escribano, 2025).

Recurrence interval of large earthquakes

Earthquake history of the Polochic–Motagua fault system. Despite its tectonic significance and in contrast to other transform plate boundaries (Fraser *et al.*, 2010; Marco and Klinger 2014; Rockwell *et al.*, 2015; Howarth *et al.*, 2018), there is a notable absence of a thorough and extensive paleoseismic record to document the earthquake history of the Polochic–Motagua fault system. In the centuries preceding the 1976 earthquake, historical records compiled from colonial archives document two seismic periods separated by extended periods of relative inactivity (White, 1984).

The first active period from 1702 to 1822 along the Polochic–Motagua fault system included 18 damaging earthquakes (White, 1984). This period culminated with a rupture of the eastern portion of the Polochic fault in 1785 (magnitude 7.3–7.5, ~175–220 km rupture length) and the western portion in 1816 (magnitude 7.5–7.7, ~240 km rupture length), followed by 5 yr of regional aftershocks through 1821 (Fig. 3; White, 1984). The 1816 event represents the largest earthquake in Guatemala's historical record based on the extent of intensity VII damage (White, 1984). This active period was preceded by a quiescent period extending from ~1560 to 1702, when no damaging earthquakes with magnitudes >6.0 (estimated) were recorded despite reasonably complete historical documentation (White, 1984; Peraldo and Montero, 1999; Peruzza *et al.*, 2021, 2023).

After 1821, the Polochic–Motagua fault system entered a second quiescent period of 123 yr with no damaging earthquakes (estimated magnitude >6.0) documented through instrumental and historical records (White, 1984). The 1945 Quiriguá earthquake on the Motagua fault, near the later epicenter of the 1976 earthquake, marked the beginning of a second active period that culminated with the 1976 Motagua fault rupture (White, 1984).

Beyond colonial and historical documentation of earthquakes (White, 1984; White and Harlow, 1993), lake sediment analysis at Lake Chichój is consistent with irregular seismic activity over 1200 yr (Fig. 7; Brocard *et al.*, 2014, 2016). This record was interpreted to show a distinct cluster of four earthquakes from ~750 to 1000 C.E., moderate activity from ~1000 to 1450 C.E., and a 500 yr quiescence from ~1450 C.E. until the 1976 event. The Lake Chichój record also provides evidence for mixed seismic and aseismic deformation processes along the Polochic fault, with meter-scale creep interpreted during seismically quiescent periods between 1665 and 1976 C.E. (Brocard *et al.*, 2016). Trenches along the Polochic fault provide additional evidence of past seismicity. At least five surface-rupturing earthquakes occurred during the past 17,000 yr, yielding minimum-average recurrence intervals of 3300–4300 yr for large earthquakes (Authemayou *et al.*, 2012).

Additional estimates of recurrence along the Polochic–Motagua fault system are uncertain. When the late Quaternary slip rates (1.5–6.0 mm/yr for the Motagua fault) are combined with the average 1.1 m displacement from the 1976 earthquake, estimated recurrence intervals for large surface-rupturing earthquakes range from 180 to 755 yr (Schwartz *et al.*, 1979). The limited number of trenching investigations, constraining observations to a single location, may not reflect system-wide behavior, particularly given evidence for strain partitioning across multiple parallel fault traces. In addition, age constraints for Quaternary features, such as those investigated by Schwartz *et al.* (1979), remain poor across the wide temporal ranges typical of standard dating methods, contributing to the substantial uncertainty in slip-rate determination. Variation in recurrence estimates for the main faults of the plate boundary, from 180 to 755 yr (geological; Schwartz *et al.*, 1979) to ~160 to 280 yr (Plafker, 1976; White 1984) representing the duration of regional quiescent periods between major transform-fault earthquakes, to 3300–4400 yr (paleoseismic evidence; Authemayou *et al.*, 2012), reflects both methodological uncertainties and complexity in fault system behavior.

Modeling the Polochic–Motagua fault system. Slip deficit rate modeling identifies locked asperities that correspond to historical rupture locations, including the 1976 Motagua, 1816 northern Polochic, and 1785 southern Polochic earthquake zones, providing evidence that current strain accumulation patterns reflect persistent structural controls on rupture behavior (Maurer *et al.*, 2025). The segment that ruptured in 1976 currently exhibits slip deficit rates of 8–10 mm/yr along the eastern Motagua fault, decreasing systematically westward. This spatial pattern of contemporary strain accumulation differs from the 1976 rupture characteristics, for which maximum moment release and surface displacement occurred in the western portions of the rupture despite lower present-day strain accumulation rates in those areas. Modeling suggests that the 1976 earthquake released strain that had accumulated over multiple centuries following the last major Motagua fault rupture, consistent with the extended quiescent period documented in historical records (White, 1984).

Estimates of contemporary Polochic fault slip rates vary substantially among modeling approaches. Whereas earlier geodetic studies indicated slip rates of 3.1–3.3 mm/yr (Ellis *et al.*, 2019), recent elastic slip deficit rate modeling suggests ~6–7 mm/yr (Maurer *et al.*, 2025). However, finite-element modeling that incorporates crustal strain yields intermediate values of 3–4 mm/yr for most of the fault length (Maurer *et al.*, 2025), more consistent with earlier estimates. The higher slip deficit rates may reflect model assumptions about fault locking or elastic behavior that do not fully capture the complexity of strain accommodation across the fault system. These discrepancies highlight remaining uncertainties in quantifying how contemporary strain accumulation is partitioned between the Motagua and Polochic faults and across minor fault segments that collectively contribute 1–3 mm/yr to total plate boundary motion.

Moment deficit rate calculations provide direct estimates of earthquake potential across the entire plate boundary zone. Geodetic models yield moment deficit rates of $0.66–1.3 \times 10^{19}$ N · m/yr for the entire region, depending on assumed elastic crustal thickness and modeling approach, values that exceed estimated moment release rates from historic earthquakes since 1560 ($0.21–0.37 \times 10^{19}$ N · m/yr; White, 1984; Maurer *et al.*, 2025). This discrepancy may be due to an incomplete earthquake catalog or moment release through other means than earthquakes, including postseismic creep and inelastic processes such as folding.

Recurrence time of the 1976 Motagua-style earthquake. Estimating recurrence intervals for earthquakes similar to the 1976 event requires reconciling the mean surface rupture of 1.1 m (Plafker *et al.*, 1976) or 2 m at depth (Kanamori and Stewart, 1978) with spatially variable contemporary slip rates. Using average slip deficit rates of 8–10 mm/yr for the eastern Motagua fault yields recurrence estimates of 110–250 yr for that segment, but the lower rates documented in western portions (~2 to 3 mm/yr) for which maximum 1976 displacement occurred suggest intervals of 300–1000 yr. These calculations assume uniform seismic strain release and do not account for the documented complexity in rupture behavior.

The moment deficit calculations provide an alternative constraint on recurrence timescales. If the 1976 earthquake released ~2.1 to 3.7×10^{20} N · m and contemporary moment accumulation rates on the ruptured segment of the Motagua fault are ~2.16 to 2.25×10^{18} N · m/yr (Maurer *et al.*, 2025), a complete repetition of the 1976 rupture would require ~100 to 170 yr of strain accumulation at current rates. This range is smaller than the 180–755 yr estimates derived from late Quaternary geological slip rates combined with 1976 displacement measurements (Schwartz *et al.*, 1979) and overlaps with the ~160 to 280 yr period between major transform-fault earthquakes on the Polochic–Motagua fault system (Plafker, 1976; White, 1984). Polochic fault slip rates (3–7 mm/yr depending on modeling approach) affect these system-wide estimates because strain partitioning between the parallel fault strands influences how quickly each structure approaches failure.

The concentration of coseismic slip and moment release in the western portions of the 1976 rupture, for which contemporary strain accumulation rates are lower, presents a significant complication. This pattern may indicate that individual fault segments do not rupture uniformly during each earthquake cycle (Dolan *et al.*, 2024). Eastern segments experiencing higher contemporary strain rates may fail through more frequent moderate magnitude events, through different rupture scenarios, or through creep, than the complete fault failure observed in 1976. Alternatively, the eastern segments may be approaching failure conditions faster than the western portions, potentially leading to partial ruptures that differ substantially from the 1976 event in both magnitude and spatial extents.

The limited historical record provides minimal constraint on characteristic Motagua fault rupture behavior. No large Motagua fault earthquakes are documented between 1560 and 1976, representing a single interevent period insufficient to establish typical recurrence patterns (White, 1984). White's historical record could also be incomplete, misattributing events to the subduction zone that could have occurred on the Motagua fault (e.g., Peraldo and Montero, 1999). Nevertheless, whether the 400 yr interval between 1560 and 1976 represents a characteristic recurrence time or an anomalously long period remains unresolved. The presence of locked asperities corresponding to historical rupture zones (Maurer *et al.*, 2025) suggests that contemporary strain accumulation may preferentially load the same fault segments, supporting the possibility of characteristic rupture behavior. However, the temporal switching of major seismic activity between the Motagua and Polochic fault structures over timescales of centuries (White, 1984) indicates that the system does not maintain constant behavior between earthquake cycles. This phenomenon,

documented across multiple fault systems globally, potentially reflects how parallel faults within plate boundary zones can trade off slip in time and space to accommodate relative plate motions (Dolan *et al.*, 2024).

LESSONS LEARNED AND IMPLICATIONS FOR FUTURE EARTHQUAKES

The 1976 Motagua earthquake and the past five decades of scientific investigations demonstrate that seismic hazard assessment for the North American–Caribbean plate boundary requires evaluation of the fault system as an integrated whole rather than treatment of individual structures as independent sources. The Motagua and Polochic faults cannot be assessed in isolation from the broader plate boundary extending offshore to the Swan fault and southward into the western Caribbean plate extensional zone.

Hazard models based on contemporary geodetic strain accumulation mischaracterize earthquake probability on parallel fault strands. The current dominance of the Motagua fault in accommodating plate motion (Franco *et al.*, 2012; Ellis *et al.*, 2019; Maurer *et al.*, 2025) does not preclude future large earthquakes on the Polochic fault, which hosted the largest documented historical earthquake despite presently accumulating minimal geodetic strain (White, 1984; Franco *et al.*, 2012). Temporal switching of major seismic activity between these structures over centuries (White, 1984) indicates fault segments can remain quiet while accumulating stress through mechanisms not captured by short-term geodetic monitoring. Probabilistic assessments must assign nonnegligible earthquake probabilities to both principal faults regardless of contemporary strain partitioning.

Stress transfer requires that earthquake scenarios consider cascading effects and mechanical interactions between fault segments. The demonstrated coupling between offshore Swan fault ruptures and the Motagua fault (Graham *et al.*, 2012) indicates that large earthquakes anywhere along the plate boundary alter stress conditions on adjacent structures, similar to other strike-slip plate boundaries (Stein *et al.*, 1997). Hazard assessments based on characteristic earthquake models for individual faults will underestimate the probability of triggered or time-clustered events.

Ground-motion prediction for Guatemala City and other population centers must account for rupture directivity effects rather than relying solely on distance-based attenuation. The concentration of damage in areas along the rupture propagation path (Fig. 7; Espinosa *et al.*, 1976), despite greater epicentral distances (Kanamori and Stewart, 1978; Harp *et al.*, 1981; Young *et al.*, 1989; Obrist-Farner *et al.*, 2025), demonstrates that standard models may substantially underestimate shaking intensity for directivity-favorable locations (e.g., Somerville *et al.* 1997; Spudich and Chiou, 2008). This applies particularly to infrastructure and population centers along the probable rupture direction for potential future events.

Extensive activation of secondary faults during the 1976 earthquake (Plafker *et al.*, 1976; Langer and Bollinger, 1979; White and Harlow, 1979) indicates that seismic hazard extends across a zone tens of kilometers wide. The Guatemala City graben and other extensional structures (Rodriguez *et al.*, 2009; Ellis *et al.*, 2019; Garnier *et al.*, 2022) represent active sources capable of generating damaging earthquakes independently or as triggered events (e.g., the 1917 Guatemala earthquake; Morley, 1918). Urban planning must address hazard from both distant large earthquakes on the Motagua or Polochic faults and proximal moderate earthquakes on secondary structures.

The incomplete paleoseismic record (Authemayou *et al.*, 2012; Brocard *et al.*, 2016) and large uncertainties in recurrence estimates (Schwartz *et al.*, 1979; White, 1984; Maurer *et al.*, 2025) indicate deterministic forecasts remain unreliable. However, the demonstrated capacity of both faults to generate large earthquakes, evidence for fault interaction, and documented temporal clustering (White, 1984) suggest the system concentrates seismic hazard over intervals separated by extended quiescent periods. The sequence of major earthquakes on the Swan fault since 2009 (Fig. 3; Graham *et al.*, 2012; Cheng and Wang, 2020; Calais *et al.*, 2025) combined with the absence of large onshore events since 1976 raises questions about stress accumulation and potential progressive failure, analogous to cascading sequences along the North Anatolian fault (Stein *et al.*, 1997). Comprehensive Coulomb stress analysis across the entire plate boundary is needed to quantify how offshore ruptures and the 1976 event have altered loading conditions and whether current stress conditions favor near-term ruptures on onshore structures.

These considerations require that seismic hazard assessment, building codes, and emergency planning for Guatemala treat the entire plate boundary as an interconnected system. Following the 1976 earthquake, Guatemala implemented improved building codes through standards established by the Guatemalan Association of Structural and Seismic Engineering (AGIES—Normas de Seguridad Estructural Para Guatemala). However, a large proportion of structures remain noncompliant with these recommendations (fig. 2 in Orihuela *et al.*, 2025), leaving substantial portions of the population vulnerable. The patterns of rupture behavior, ground-motion distribution, and secondary fault activation documented in 1976 demonstrate that future large earthquakes will expose significant proportion of Guatemalan society to severe seismic risk. This vulnerability is compounded by rapid population growth and ongoing infrastructure expansion in a developing country, which complicate efforts to implement comprehensive seismic zoning and enforce building standards.

FUTURE RESEARCH NEEDS

Further analysis of the 1976 Motagua earthquake, in combination with contemporary studies of the Polochic–Motagua fault system, will continue to advance our scientific understanding

of this plate boundary. Ultimately, better scientific understanding and characterization of seismicity along the Polochic–Motagua fault system will lead to better seismic hazard assessments for the region. We highlight several avenues for scientific research that can be used to improve hazard maps (e.g., Benito *et al.*, 2012; Gamboa-Canté *et al.* 2025) to better characterize risk along this multifault system.

1. Compared with other transform plate boundaries (e.g., San Andreas fault; McPhillips, 2022), the paleoseismic record along the Polochic–Motagua fault system is limited (Authemayou *et al.*, 2012; Brocard *et al.*, 2016). Systematic paleoseismic studies, including on-fault trenching and lacustrine paleoseismic investigations, are required to constrain earthquake recurrence patterns, fault switching behavior, and temporal clustering of seismic activity.
2. Improved quantification of long-term slip rates through geological studies of offset features and dating past earthquakes at more locations throughout the fault system will help characterize the seismic hazard of individual fault strands. Uncertainties remain regarding the activity and slip rates of structures such as the Jocotán–Chamelecón fault zone and the Ixcán fault, which may accommodate portions of plate boundary motion despite limited seismic activity.
3. Expansion of permanent seismic networks and geodetic monitoring capabilities is essential for improving hazard assessment in Guatemala. Improved instrumentation capabilities will help characterize contemporary deformation patterns and strain accumulation across the entire region, increasing the resolution of distributed deformation across multiple fault strands (González-Negreros and Gaspar-Escribano, 2025). Although an early warning system has now been established in Guatemala (e.g., Orihuela *et al.*, 2025) and could provide tens of seconds of advanced notice if a similar 1976 earthquake were to occur (e.g., Orihuela *et al.*, 2023), the lack of high-density instrumentation coverage prevents system efficiency. Current efforts to enhance instrumentation coverage include the Lake Izabal seismic array and the International Continental Scientific Drilling Program Lake Izabal Basin Research Endeavor project (Obrist-Farner *et al.*, 2023).
4. To better understand distributed deformation across the Polochic–Motagua fault system, comprehensive mapping of fault traces and determination of their activity through enhanced seismic monitoring and additional Global Navigation Satellite Systems and Interferometric Synthetic Aperture Radar (InSAR) studies is essential. Current studies lack consistency regarding which structures are active, with disagreement about the role of secondary faults in accommodating plate motion (Guzmán-Speziale and Molina, 2022; Agate *et al.*, 2024; Maurer *et al.*, 2025). The recognition that minor fault segments accommodate slip (Maurer *et al.*, 2025) highlights the need for additional investigations to distinguish active fault strands from inactive structures and quantify their contributions to total strain accommodation. Modern remote sensing techniques, including expanding light detection and ranging (lidar) coverage (currently limited to two locations along the Motagua fault; Fig. 9) and InSAR investigations, can improve fault-trace geometry, confirm uncertain structures, and integrate geomorphic and subsurface observations into unified fault maps.
5. More advanced source modeling for the 1976 event is needed to better resolve the source complexity seen in earlier modeling studies (Kanamori and Stewart, 1978; Kikuchi and Kanamori, 1982, 1991; Young *et al.*, 1989) to understand subevents, moment release, earthquake magnitude, and rupture directivity and how these processes affected ground acceleration and consequent building damage. Additional details on rupture heterogeneity and propagation dynamics through the analysis of digitized waveforms from the 1976 earthquake and the use of modern computational capabilities can help resolve these discrepancies. Waveforms preserved through the Albuquerque Seismological Lab WWSSN Film Chip Preservation Project (Alejandro *et al.*, 2019) provide access to teleseismic records that can be examined using contemporary inversion techniques and higher-resolution analysis methods not available during initial investigations.
6. Provide quantitative constraints for probabilistic seismic hazard assessment across the North American–Caribbean transform system. This is important given that the plate boundary since 1976 has ruptured in a predictive pattern (Fig. 3) similar to observations from the North Anatolian fault (e.g., Stein *et al.*, 1997). Such modeling should evaluate how the sequence of Swan fault ruptures since 2009, combined with the 1976 Motagua earthquake and historical Polochic fault events, has modified loading conditions on all fault segments within the system.
7. Understanding the structural framework that governs fault behavior, rupture dynamics, and the distribution of deformation across the Polochic–Motagua fault system requires comprehensive geological mapping. The most recent nationwide geologic map of Guatemala (Bonis *et al.*, 1970) remains a critical reference but lacks the stratigraphic and structural resolution necessary for comprehensive tectonic and hazard analyses. Subsequent studies have highlighted significant geological complexities, especially along the Motagua valley (Brueckner *et al.*, 2009; Angiboust *et al.*, 2021; Harlow *et al.*, 2025), which can help establish constraints on crustal architecture that controls fault localization and strain partitioning.

CONCLUSION

The 1976 Motagua earthquake established the significance of the Motagua Fault as part of the North American and Caribbean

plate boundary. The event exhibited an asymmetric bilateral rupture with strongly westward-directed moment release and substantial spatial variations in slip and destruction. Although surface displacements were significant, seismological inversion models showed higher coseismic slip magnitudes at depth. Beyond the primary rupture, extensive secondary faulting and aftershock activity showcased the complexity of the fault system. Five decades of investigations have illuminated fundamental uncertainties of this plate boundary and its associated hazard. Current recurrence estimates do not allow to quantify how often large earthquake occur, and the fault strands of the plate boundary with high seismic risk are unknown. Understanding this plate boundary requires continued monitoring infrastructure and efforts currently inadequate for a fault system capable of producing large earthquakes of $M_w > 7$. The preservation of legacy data from the 1976 earthquake, in combination with continued scientific investigations and expansion of monitoring capabilities in Guatemala, will provide the foundation for integrated hazard assessment along the North American–Caribbean plate boundary.

DATA AND RESOURCES

All supplemental material, including original topographic maps with field annotations; aerial photographs spanning the western and central segments of the surface rupture; 35 mm color photographs taken by the U.S. Geological Survey (USGS) team during the 1976 expedition; field notebooks containing detailed observations, measurements, and sketches; and previously published aftershock datasets converted to standardized digital formats, are available digitally (McEnaney and Clark, 2025).

DECLARATION OF COMPETING INTERESTS

The authors acknowledge that there are no conflicts of interest recorded.

ACKNOWLEDGMENTS

This work was supported by the U.S. National Science Foundation (NSF) Award EAR-2038179 and EAR-2305799. The authors thank Associate Editor Thomas M. Brocher and Editor-in-Chief Martin Mai for insightful comments that significantly improved the quality of this article.

REFERENCES

Agate, M., F. Caldareri, L. Castillo, A. Garcia, G. Giunta, L. Mixco, J. Requena, C. Rubi Tellez, M. Ruiz, A. Sulli, *et al.* (2024). The pattern of brittle deformation in Central America for an assessment of the seismo-tectonic framework, *J. Maps* **20,** no. 1, 2285479, doi: 10.1080/17445647.2023.2285479.

Alejandro, A. C. B., C. R. Hutt, A. T. Ringler, S. V. Moore, R. E. Anthony, and D. C. Wilson (2019). The Albuquerque Seismological Lab WWSSN film chip preservation project, *Seismol. Res. Lett.* **90,** no. 1, 401–408, doi: 10.1785/0220180275.

Angiboust, S., J. Muñoz-Montecinos, A. Cambeses, T. Raimondo, D. Deldicque, and A. Garcia-Casco (2021). Jolts in the jade factory: A route for subduction fluids and their implications for mantle wedge seismicity, *Earth Sci. Rev.* **220,** 103720, doi: 10.1016/j.earscirev.2021.103720.

Authemayou, C., G. Brocard, C. Brocard, T. Simon-Labric, A. Guttierrez, E. N. Chiquín, and S. Morán (2011). The Caribbean-North America-Cocos Triple Junction and the dynamics of the Polochic-Motagua fault systems: Pull-up and zipper models, *Tectonics* **30,** TC3010, doi: 10.1029/2010TC002814.

Authemayou, C., G. Brocard, C. Teyssier, B. Suski, B. Cosenza, S. Morán-Ical, C. W. González-Véliz, M. A. Aguilar-Hengstenberg, and K. Holliger (2012). Quaternary seismo-tectonic activity of the Polochic fault, Guatemala, *J. Geophys. Res.: Solid Earth* **117,** B07403, doi: 10.1029/2012JB009444.

Bao, H., L. Xu, L. Meng, J. P. Ampuero, and S. Ni (2022). Global frequency of oceanic and continental supershear earthquakes, *Nature Geosci.* **15,** 942–949, doi: 10.1038/s41561-022-01055-5.

Bartole, R., E. Lodolo, J. Obrist-Farner, and D. Morelli (2019). Sedimentary architecture, structural setting, and Late Cenozoic depocentre migration of an asymmetric transtensional basin: Lake Izabal, eastern Guatemala, *Tectonophysics* **750,** 419–433, doi: 10.1016/j.tecto.2018.12.004.

Benito, M. B., C. Lindholm, E. Camacho, Á. Climent, G. Marroquín, E. Molina, W. Rojas, J. J. Escobar, E. Talavera, G. E. Alvarado, and Y. Torres (2012). A new evaluation of seismic hazard for the Central America region, *Bull. Seismol. Soc. Am.* **102,** no. 2, 504–523, doi: 10.1785/0120110015.

Bonis, S., O. Bohnenberger, and G. Dengo (compilers) (1970). Mapa geológico de la República de Guatemala, First Ed.., Instituto Geográfico Nacional, Guatemala City, scale 1:500,000, 4 sheets (in Spanish).

Brocard, G., T. Adatte, O. Magand, H. R. Pfeifer, A. Bettini, F. Arnaud, F. S. Anselmetti, and S. Morán-Icál (2014). The recording of floods and earthquakes in Lake Chichój, Guatemala, during the twentieth century, *J. Paleolimnol.* **52,** 155–169, doi: 10.1007/s10933-014-9784-4.

Brocard, G., F. S. Anselmetti, and C. Teyssier (2016). Guatemala paleoseismicity: From Late Classic Maya collapse to recent fault creep, *Sci. Rep.* **6,** 36976, doi: 10.1038/srep36976.

Brueckner, H. K., H. G. Avé Lallemant, V. B. Sisson, G. E. Harlow, S. R. Hemming, U. Martens, T. Tsujimori, and S. S. Sorensen (2009). Metamorphic reworking of a high-pressure–low-temperature mélange along the Motagua fault, Guatemala: A record of Neocomian and Maastrichtian transpressional tectonics, *Earth Planet. Sci. Lett.* **284,** 228–235, doi: 10.1016/j.epsl.2009.04.032.

Bucknam, R. C., G. Plafker, and R. V. Sharp (1978). Fault movement (afterslip) following the Guatemala earthquake of February 4, 1976, *Geology* **6,** no. 3, 170–173, doi: 10.1130/0091-7613(1978)6<170:FMAFTG>2.0.CO;2.

Caccavale, M., M. Sacchi, E. Spiga, and S. Porfido (2019). The 1976 Guatemala earthquake: ESI scale and probabilistic/deterministic seismic hazard analysis approaches, *Geosciences* **9,** no. 9, 403, doi: 10.3390/geosciences9090403.

Calais, E., B. Delouis, J.-P. Ampuero, H. Bao, F. Courboulex, A. Deschamps, B. de Lépinay, T. Monfret, L. Meng, L. Xu, *et al.* (2025). The 28 January 2020, Mw 7.7, Cayman Trough/Oriente Fault supershear earthquake rupture, *Seismica* **4,** no. 2, doi: 10.26443/seismica.v4i2.1629.

Cheng, C., and D. Wang (2020). Imaging the rupture process of the 10 January 2018 Mw 7.5 Swan Island, Honduras, earthquake, *Earthq. Sci.* **33,** no. 4, 194–200, doi: 10.29382/eqs-2020-0194-03.

DeMets, C., P. E. Jansma, G. S. Mattioli, T. H. Dixon, F. Farina, R. Bilham, E. Calais, and P. Mann (2000). GPS geodetic constraints on Caribbean–North America plate motion, *Geophys. Res. Lett.* **27,** no. 3, 437–440, doi: 10.1029/1999GL005436.

Dewey, J. W., and B. R. Julian (1976). Main event source parameters from teleseismic data, in *The Guatemalan Earthquake of February 4, 1976: A Preliminary Report*, A. F. Espinosa (Editor), *U.S. Geol. Surv. Profess. Pap. 1002*, 14–19, U.S. Geological Survey, Reston, Virginia.

Dolan, J. F., R. J. Van Dissen, E. J. Rhodes, R. Zinke, A. E. Hatem, C. McGuire, R. M. Langridge, and J. R. Grenader (2024). One tune, many tempos: Faults trade off slip in time and space to accommodate relative plate motions, *Earth Planet. Sci. Lett.* **625,** 118484, doi: 10.1016/j.epsl.2023.118484.

Ellis, A., C. DeMets, R. McCaffrey, P. Briole, B. Cosenza Muralles, O. Flores, M. Guzmán-Speziale, D. Hernández, V. Kostoglodov, P. LaFemina, *et al.* (2019). GPS constraints on deformation in northern Central America from 1999 to 2017, part 2: Block rotations and fault slip rates, fault locking and distributed deformation, *Geophys. J. Int.* **218,** no. 2, 729–754, doi: 10.1093/gji/ggz173.

Espinosa, A. F. (Editor) (1976). *The Guatemalan Earthquake of February 4, 1976: A Preliminary Report*, *U.S. Geol. Surv. Profess. Pap. 1002*, U.S. Geological Survey, Reston, Virginia, 90 pp.

Espinosa, A. F., R. Husid, and A. Quesada(1976). Intensity distribution and source parameters from field observations, in The Guatemalan Earthquake of February 4, 1976, a Preliminary Report, *U.S. Geol. Surv. Profess. Pap. 1002*, 52–66.

Franco, A., C. Lasserre, H. Lyon-Caen, V. Kostoglodov, E. Molina, M. Guzmán-Speziale, D. Monterosso, V. Robles, C. Figueroa, W. Amaya, *et al.* (2012). Fault kinematics in northern Central America and coupling along the subduction interface of the Cocos Plate, from GPS data in Chiapas (Mexico), Guatemala, and El Salvador, *Geophys. J. Int.* **189,** no. 3, 1223–1236, doi: 10.1111/j.1365-246X.2012.05390.x.

Franco, A., E. Molina, H. Lyon-Caen, J. Vergne, T. Monfret, A. Nercessian, S. Cortez, O. Flores, D. Monterosso, and J. Requenna (2009). Seismicity and crustal structure of the Polochic–Motagua fault system area (Guatemala), *Seismol. Res. Lett.* **80,** no. 6, 977–984, doi: 10.1785/gssrl.80.6.977.

Fraser, J., K. Vanneste, and A. Hubert-Ferrari (2010). Recent behavior of the North Anatolian Fault: Insights from an integrated paleoseismological data set, *J. Geophys. Res.: Solid Earth* **115,** B09408, doi: 10.1029/2009JB006982.

Gamboa-Canté, C., M. Arroyo-Solórzano, B. Benito, J. Aguilar, I. G. Arroyo, E. Camacho-Astigarrabia, D. Castro, O. Flores, L. Linkimer, M. G. Marroquín, *et al.* (2024). Seismicity in Central America (1520–2020) and earthquake catalog compilation for seismic hazard assessments, *Bull. Earthq. Eng.* **22,** 7201–7234, doi: 10.1007/s10518-024-02059-9.

Gamboa-Canté, G. A., M. Arroyo-Solórzano, A. Rivas-Medina, and M. B. Benito (2025). Overview of seismic hazard studies in Central America: A comparative analysis of results, *J. South Am. Earth Sci.* **164,** 105630, doi: 10.1016/j.jsames.2025.105630.

Garnier, B., C. DeMets, M. Kaplan, L. Sánchez, D. León, L. Mixco, and A. Staller (2022). Deformation in western Guatemala associated with the NAFCA (North America–Central American Forearc–Caribbean) triple junction: Neotectonic strain localization into the Guatemala City graben, *Tectonics* **41,** no. 2, e2021TC006739, doi: 10.1029/2021TC006739.

Garnier, B., B. Tikoff, O. Flores, B. Jicha, C. DeMets, B. Cosenza-Muralles, D. Hernandez, G. Marroquin, L. Mixco, and W. Hernandez (2021). An integrated structural and GPS study of the Jalpatagua fault, southeastern Guatemala, *Geosphere* **17,** no. 1, 201–225, doi: 10.1130/GES02243.1.

González-Negreros, R., and J. M. Gaspar-Escribano (2025). Analysis of the Guatemalan earthquake catalog, *J. Seismol.* **29,** 565–583, doi: 10.1007/s10950-025-10293-0.

Graham, S. E., C. DeMets, E. Cabral-Cano, V. Kostoglodov, A. Walpersdorf, N. Cotte, M. Brudzinski, R. McCaffrey, and L. Salazar-Tlaczani (2012). GPS constraints on the Mw 7.3 2009 Swan Islands earthquake: Remote triggering and seismic hazard in Honduras, *Geophys. J. Int.* **190,** no. 2, 1329–1338, doi: 10.1111/j.1365-246X.2012.05556.x.

Guzmán-Speziale, M., and E. Molina (2022). Seismicity and seismically active faulting of Guatemala: A review, *J. South Am. Earth Sci.* **115,** 103740, doi: 10.1016/j.jsames.2022.103740.

Harlow, G. E., K. E. Flores, C. Martin, V. B. Sisson, and S. S. Sorensen (2025). Serpentinites of the Guatemala Suture Zone: Varieties, origin, and compositional modification, *Am. J. Sci.* **325,** Art. 4, doi: 10.2475/001c.129404.

Harp, E. L., R. C. Wilson, and G. F. Wieczorek (1981). *Landslides from the February 4, 1976, Guatemala Earthquake*, *U.S. Geol. Surv. Profess. Pap. 1204-A*, U.S. Geological Survey, Reston, Virginia, 35 pp.

Hayman, N. W., N. R. Grindlay, M. R. Perfit, P. Mann, S. Leroy, and B. Mercier de Lépinay (2011). Oceanic core complex development at the ultraslow spreading Mid-Cayman Spreading Center, *Geochem. Geophys. Geosys.* **12,** Q0AG02, doi: 10.1029/2010GC003240.

Howarth, J. D., U. A. Cochran, R. M. Langridge, K. Clark, S. J. Fitzsimons, K. Berryman, and D. T. Strong (2018). Past large earthquakes on the Alpine fault: Paleoseismological progress and future directions, *New Zeal. J. Geol. Geophys.* **61,** 309–328, doi: 10.1080/00288306.2018.1464658.

Husid, R., A. F. Espinosa, and A. Quesada (1976). Damage and engineering implications, in *The Guatemalan Earthquake of February 4, 1976: A Preliminary Report*, A. F. Espinosa (Editor), *U.S. Geol. Surv. Profess. Pap. 1002*, 67–79, U.S. Geological Survey, Reston, Virginia

Kanamori, H., and G. S. Stewart (1978). Seismological aspects of the Guatemala earthquake of February 4, 1976, *J. Geophys. Res.* **83,** no. B7, 3427–3434, doi: 10.1029/JB083iB07p03427.

Kikuchi, M., and H. Kanamori (1982). Inversion of complex body waves, *Bull. Seismol. Soc. Am.* **72,** no. 2, 491–506, doi: 10.1785/BSSA0720020491.

Kikuchi, M., and H. Kanamori (1991). Inversion of complex body waves—III, *Bull. Seismol. Soc. Am.* **81,** no. 6, 2335–2350, doi: 10.1785/BSSA0810062335.

Kusky, T. M., P. Mann, and J. Meng (2025). The February 8, 2025, Swan Islands (Caribbean Sea) earthquake: Lessons for geohazards on transform plate and microplate boundaries, *J. Earth Sci.* **36,** 852–855, doi: 10.1007/s12583-025-0176-7.

Langer, C. J., and G. A. Bollinger (1979). Secondary faulting near the terminus of a seismogenic strike-slip fault: Aftershocks of the 1976

Guatemala earthquake, *Bull. Seismol. Soc. Am.* **69,** no. 2, 427–444, doi: 10.1785/BSSA0690020427.

Langer, C. J., J. H. Whitcomb, and A. Q. Aburto (1976). Aftershocks from local data, in *The Guatemalan Earthquake of February 4, 1976: A Preliminary Report*, A. F. Espinosa (Editor), *U.S. Geol. Surv. Profess. Pap. 1002*, U.S. Geological Survey, Reston, Virginia, 26–37.

Lisowski, M., and W. Thatcher (1981). Geodetic determination of horizontal deformation associated with the Guatemala earthquake of 4 February 1976, *Bull. Seismol. Soc. Am.* **71,** no. 3, 845–856, doi: 10.1785/BSSA0710030845.

Lyon-Caen, H., E. Barrier, C. Lasserre, A. Franco, I. Arzu, L. Chiquin, M. Chiquin, T. Duquesnoy, O. Flores, O. Galicia, *et al.* (2006). Kinematics of the North American–Caribbean–Cocos plates in Central America from new GPS measurements across the Polochic–Motagua fault system, *Geophys. Res. Lett.* **33,** no. 19, doi: 10.1029/2006GL027694.

Marco, S., and Y. Klinger (2014). Review of on-fault paleoseismic studies along the Dead Sea Fault, in *Dead Sea Transform Fault System: Reviews*, Z. Garfunkel, Z. Ben-Avraham, and E. Kagan (Editors), Vol. 6, Springer, Dordrecht, The Netherlands, 183–205, doi: 10.1007/978-94-017-8872-4_7.

Matumoto, T., and G. V. Latham (1976). Aftershocks of the Guatemalan earthquake of February 4, 1976, *Geophys. Res. Lett.* **3,** no. 10, 599–602, doi: 10.1029/GL003i010p00599.

Maurer, J., A. Eckert, and Q. Sun (2025). Deformation and earthquake potential on the North America–Caribbean–Cocos triple junction in Guatemala, *ESS Open Archive*, 24 July 2025, doi: 10.22541/essoar.175336982.28467707/v1.

McEnaney, T., and G. Clark (2025). 1976 Motagua Earthquake georeferenced database (1.0.0) [Data set], *Zenodo* doi: 10.5281/zenodo.17674716.

McPhillips, D. (2022). Revised earthquake recurrence intervals in California, U.S.A.: New paleoseismic sites and application of event likelihoods, *Seismol. Res. Lett.* **93,** no. 6, 3009–3023, doi: 10.1785/0220220127.

Molnar, P., and L. R. Sykes (1969). Tectonics of the Caribbean and Middle America regions from focal mechanisms and seismicity, *Geol. Soc. Am. Bull.* **80,** no. 9, 1639–1684, doi: 10.1130/0016-7606(1969)80[1639:TOTCAM]2.0.CO;2.

Morley, S. (1918). The Guatemala earthquake of December, 1917 and January, 1918, *The Geograph. Rev.* **6,** 459–469.

Muehlberger, W. R., and A. W. Ritchie (1975). Caribbean–Americas plate boundary in Guatemala and southern Mexico as seen on Skylab IV orbital photography, *Geology* **3,** no. 5, 232–235, doi: 10.1130/0091-7613(1975)3.

Obrist-Farner, J., A. Eckert, P. M. J. Douglas, L. Perez, A. Correa-Metrio, B. L. Konecky, T. Bauersachs, S. Zimmerman, S. Scheidt, M. Brenner, *et al.* (2023). Planning for the Lake Izabal Basin Research Endeavor (LIBRE) continental scientific drilling project in eastern Guatemala, *Sci. Drill.* **32,** 85–95, doi: 10.5194/sd-32-85-2023.

Obrist-Farner, J., A. Eckert, M. Locmelis, J. L. Crowley, B. Mota-Vidaure, E. Lodolo, J. Rosenfeld, and E. Duarte (2020). The role of the Polochic Fault as part of the North American and Caribbean Plate boundary: Insights from the infill of the Lake Izabal Basin, *Basin Res.* **32,** no. 1, 73–92, doi: 10.1111/bre.12431.

Obrist-Farner, J., J. Maurer, D. Gibson, T. McEnaney, A. Eckert, W. F. Kenney, J. Beeson, N. Wattrus, Q. Stangeland, and F. Reyes (2025). Paleoseismic evidence of directivity for the 1976 Mw 7.5 Motagua earthquake, Guatemala, *Geology* **53,** no. 11, 971–976, doi: 10.1130/G53449.1.

Orihuela, B., I. Dallo, J. Clinton, W. Strauch, M. Protti, R. Yani, G. Marroquín, J. Sanchez, F. Vega, M. Marti, *et al.* (2023). Earthquake early warning in Central America: The societal perspective, *Int. J. Disast. Risk Reduc.* **97,** doi: 10.1016/j.ijdrr.2023.103982.

Orihuela, B., A. N. Papadopoulos, J. Clinton, G. Marroquin, M. Protti, W. Strauch, R. Yani-Quiyuch, L. Danciu, and S. Wiemer (2025). Impact assessment of earthquake early warning systems in Central America, *Earthq. Spectra* **41,** no. 4, 3094–3122, doi: 10.1177/87552930251342826.

Peraldo, G., and W. Montero (1999). Sismología histórica de América Central, Instituto Panamericano de Geografía e Historia, México, 346 pp. (in Spanish).

Peruzza, L., E. Esposito, F. E. Rodríguez García, R. A. García Castro, P. Santos, G. Marroquín, L. Mixco, L. Torres Bernhard, R. Torres, D. A. Hernandez, *et al.* (2021). MARCA-GEHN, a prototype macroseismic archive of four Central America countries, *Boll. Geof. Teor. Appl.* **62,** no. s2, 3–196.

Peruzza, L., E. Esposito, F. E. Rodríguez García, and G. Giunta (2023). *A Tool for Archiving and Updating Knowledge About Past Earthquakes in Central America*, IntechOpen, published 15 December 2023, doi: 10.5772/intechopen.1003080.

Person, W. J., W. Spence, and J. W. Dewey (1976). Main event and principal aftershocks from teleseismic data, in *The Guatemalan Earthquake of February 4, 1976: A Preliminary Report*, A. F. Espinosa (Editor), *U.S. Geol. Surv. Profess. Pap. 1002*, 1–13, U.S. Geological Survey, Reston, Virginia.

Plafker, G. (1976). Tectonic aspects of the Guatemala earthquake of 4 February 1976, *Science* **193,** no. 4259, 1201–1208, doi: 10.1126/science.193.4259.1201.

Plafker, G., M. G. Bonilla, and S. B. Bonis (1976). Geologic effects, in *The Guatemalan Earthquake of February 4, 1976: A Preliminary Report*, A. F. Espinosa (Editor), *U.S. Geol. Surv. Profess. Pap. 1002*, U.S. Geological Survey, Reston, Virginia, 38–51.

Rockwell, T. K., T. E. Dawson, J. Young Ben-Horin, and G. Seitz (2015). A 21-event, 4,000-year history of surface ruptures in the Anza seismic gap, San Jacinto Fault, and implications for long-term earthquake production on a major plate boundary fault, *Pure Appl. Geophys.* **172,** 1143–1165, doi: 10.1007/s00024-014-0955-z.

Rodriguez, M., C. DeMets, R. D. Rogers, C. Tenorio, D. Hernandez, P. Hernandez, E. Molina, and A. Correa-Metrio (2009). A GPS and modelling study of deformation in northern Central America, *Geophys. J. Int.* **178,** no. 3, 1733–1754, doi: 10.1111/j.1365-246X.2009.04251.x.

Scholz, C. H., M. Wyss, and S. W. Smith (1969). Seismic and aseismic slip on the San Andreas Fault, *J. Geophys. Res.* **74,** no. 8, 2049–2069, doi: 10.1029/JB074i008p02049.

Schwartz, D. P. (1976). Geology of the Zacapa Quadrangle and vicinity, Guatemala, Central America, *Ph.D. Thesis*, State University of New York, Binghamton, 191 pp.

Schwartz, D. P., L. S. Cluff, and T. W. Donnelly (1979). Quaternary faulting along the Caribbean–North America plate boundary in

Central America, *Tectonophysics* **52,** nos. 1/4, 431–445, doi: 10.1016/0040-1951(79)90258-0.

Seed, H. B., R. G. Ascoli, A. Gomez-Masso, C. K. Chan, and I. Arango (1981). Earthquake-induced liquefaction near Lake Amatitlán, Guatemala, *J. Geotech. Eng. Div.* **107,** no. 4, 501–518, doi: 10.1061/AJGEB6.0001122.

Somerville, P. G., N. F. Smith, R. W. Graves, and N. A. Abrahamson (1997). Modification of empirical strong ground motion attenuation relations to include the amplitude and duration effects of rupture directivity, *Seismol. Res. Lett.* **68,** no. 1, 199–222, doi: 10.1785/gssrl.68.1.199.

Spudich, P., and B. S. J. Chiou (2008). Directivity in NGA earthquake ground motions: Analysis using isochrone theory, *Earthq. Spectra* **24,** 279–298, doi: 10.1193/1.2928225.

Stein, R. S., A. A. Barka, and J. H. Dieterich (1997). Progressive failure on the North Anatolian fault since 1939 by earthquake stress triggering, *Geophys. J. Int.* **128,** no. 3, 594–604, doi: 10.1111/j.1365-246X.1997.tb05321.x.

Styron, R., and M. Pagani (2020). The GEM global active faults database, *Earthq. Spectra* **36,** no. 1 (suppl.), 160–180, doi: 10.1177/8755293020944182.

Thingbaijam, K. K. S., P. Martin Mai, and K. Goda (2017). New empirical earthquake source-scaling laws, *Bull. Seismol. Soc. Am.* **107,** 2225–2246, doi: 10.1785/0120170017.

U.S. Geological Survey (2025). U.S. Geological Survey Earthquake Catalog and ShakeMap Products, peak ground acceleration (PGA) and Modified Mercalli Intensity (MMI) contours for the 4 February 1976 Guatemala, 8 May 2009 Swan Islands, 10 January 2018 Swan Islands, and 12 March 2025 Swan Islands earthquakes, available at https://earthquake.usgs.gov (last accessed November 2025).

Utsu, T. (1961). A statistical study on the occurrence of aftershocks, *Geophys. Mag.* **30,** 521–605.

Wells, D. L., and K. J. Coppersmith. (1994). New empirical relationships among magnitude, rupture length, rupture width, rupture area, and surface displacement, *Bull. Seismol. Soc. Am.* **84,** no. 4, 974–1002, doi: 10.1785/BSSA0840040974.

White, R. A. (1984). Catalog of historic seismicity in the vicinity of the Chixoy–Polochic and Motagua faults, Guatemala, *U.S. Geol. Surv. Open-File Rept. 84-88*, doi: 10.3133/ofr8488.

White, R. A., and D. H. Harlow (1979). Preliminary catalog of aftershocks of the Guatemala earthquake of February 4, 1976, from the area between Guatemala City and Lake Atitlan, *U.S. Geol. Surv. Open-File Rept. 79-864*, doi: 10.3133/ofr79864.

White, R. A., and D. H. Harlow (1993). Destructive upper-crustal earthquakes of Central America since 1900, *Bull. Seismol. Soc. Am.* **83,** no. 4, 1115–1142, doi: 10.1785/BSSA0830041115.

Yani-Quiyuch, R., L. Asturias, and D. Castro (2023). The rupture plane of the February 2022 Mw 6.2 Guatemala, intermediate depth earthquake, *Seismica* **2,** no. 2, doi: 10.26443/seismica.v2i2.691.

Young, C. J., T. Lay, and C. S. Lynnes (1989). Rupture of the 4 February 1976 Guatemalan earthquake, *Bull. Seismol. Soc. Am.* **79,** no. 3, 670–689, doi: 10.1785/BSSA0790030670.

Manuscript received 1 December 2025
Published online 17 February 2026